HHS Public Access

Author manuscript

J Immunol. Author manuscript; available in PMC 2021 September 15.

Published in final edited form as:

J Immunol. 2021 March 15; 206(6): 1372–1384. doi:10.4049/jimmunol.2000765.

Agonistic anti-CD40 overcomes T cell exhaustion induced by chronic myeloid cell IL-27 production in a pancreatic cancer preclinical model

Adam L. Burrack[1,2], **Meagan R. Rollins**[1,2], **Ellen J. Spartz**[1,2], **Taylor D. Mesojednik**[1,2], **Zoe C. Schmiechen**[1,2], **Jackson F. Raynor**[1,2], **Iris Wang**[1,2], **Ross M. Kedl**[3], **Ingunn M. Stromnes**[1,2,4,5,*]

[1]Department of Microbiology and Immunology, University of Minnesota Medical School, Minneapolis, MN 55414

[2]Center for Immunology, University of Minnesota Medical School, Minneapolis, MN 55415, United States

[3]University of Colorado Anschutz Medical Center, Department of Immunology & Microbiology, Aurora, CO 80045, United States

[4]Masonic Cancer Center, University of Minnesota Medical School, Minneapolis, MN 55414, United States

[5]Center for Genome Engineering, University of Minnesota Medical School, Minneapolis, MN 55414, United States

Abstract

Pancreatic cancer is a particularly lethal malignancy and resists immunotherapy. Here, using a preclinical pancreatic cancer murine model, we demonstrate a progressive decrease in IFNγ and Granzyme B and a concomitant increase in Tox and IL-10 in intratumoral tumor-specific T cells. Intratumoral myeloid cells produced elevated IL-27, a cytokine that correlates with poor patient outcome. Abrogating IL-27 signaling significantly decreased intratumoral Tox+ T cells and delayed tumor growth yet was not curative. Agonistic αCD40 decreased intratumoral IL-27-producing myeloid cells, decreased IL-10-producing intratumoral T cells, and promoted intratumoral Klrg1+Gzmb+ short-lived effector T cells. Combination agonistic αCD40+αPD-L1 cured 63% of tumor-bearing animals, promoted rejection following tumor re-challenge and correlated with a 2-log increase in pancreas-residing tumor-specific T cells. Interfering with *Ifngr1* expression in non-tumor/host cells abrogated agonistic αCD40+αPD-L1 efficacy. In contrast, interfering with non-tumor/host cell *Tnfrsf1a* led to cure in 100% of animals following agonistic αCD40+αPD-L1 and promoted the formation of circulating central memory T cells rather than

[*]**Lead Contact:** Ingunn M. Stromnes, Ph.D., University of Minnesota, Center for Immunology, Center for Genome Engineering, University of Minnesota, 2101 6th Street, MBB 2-186, Minneapolis, MN 55455, Phone: 1-612-626-7771, ingunn@umn.edu.

AUTHOR CONTRIBUTIONS

A.L.B. and I.M.S designed the study, analyzed the data, and wrote the manuscript. A.L.B., M.R.R., E.J.S., T.D.M, Z.C.S, J.F.R. and I.W. conducted experiments and analyzed data. R.M.K. provided expertise on IL-27 signaling and the IL-27 reporter strain. I.M.S is guarantor of the study.

long-lived effector T cells. In summary, we identify a mechanistic basis for T cell exhaustion in pancreatic cancer and a feasible clinical strategy to overcome it.

Keywords

Cancer; immunotherapy PDA; T cells; exhaustion PD1; CD40; IL-27; TNFα

INTRODUCTION

Pancreatic ductal adenocarcinoma (PDA), the most common form of pancreatic cancer, is currently the third leading cause of cancer-related mortality (1). PDA is often surgically inoperable at the time of diagnosis due to locally advanced and/or metastatic disease. Aggressive cytoreductive therapies confer modest improvements in overall survival (2, 3). Immune checkpoint blockade (*e.g.*, αPD-1/αPD-L1/αCTLA-4) is an attractive approach because of clinical benefit in other malignancies (4). However, PDA is largely refractory to immune checkpoint blockade and while objective responses can occur in rare PDAs with a high tumor mutational burden, such responses are often transient (5, 6). Combination of PD-1 and CTLA-4 inhibition also had minimal benefit in Phase 2 clinical trial (7).

PD-1 blockade efficacy is enhanced by modifying the suppressive tumor microenvironment (TME) in preclinical PDA animal models (8–10). One promising TME-modulating strategy is agonistic αCD40, which promotes anti-tumor myeloid cells (11) and engages T cells (12–15). Notably, agonistic αCD40 (11) similar to our engineered T cell therapy targeting mesothelin (16) promotes destruction of the fibroinflammatory tumor stroma. A combination of agonistic αCD40, αPD-1 and chemotherapy are showing promising clinical results in advanced PDA (17). Previously, we identified that a single dose of agonistic αCD40 enhanced the longevity of engineered T cells in a *Kras*$^{G12D/+}$;*Trp53*$^{R172H/+}$;*p48*-Cre (*KPC*) genetically engineered PDA mouse model (18). However, the mechanism(s) underlying agonistic αCD40 action in PDA are unclear, in part because it is often studied in combination with other immune modulatory and cytotoxic therapies. Additionally, as there are currently no identified endogenous immunogenic epitopes identified in *KPC* animals (19), few studies have distinguished a tumor antigen-specific T cell response.

We previously developed a PDA animal model that expresses a tumor-specific antigen click beetle red luciferase (CB) (20). Unlike ovalbumin, which causes *KPC* cell line rejection in syngeneic B6 mice (19, 20), *KPC* CB+ tumors grow in B6 mice and $CB_{101–109}$:H-2D^{b}-specific T cells accumulate intratumorally but are rendered defective in IFNγ and TNFα following antigen stimulation (20), consistent with differentiation into exhausted T cells (T_{EX}). In the current study, we further characterize and quantify T_{EX} formation in pancreatic cancer and identify a novel combinatorial approach to overcome T_{EX} leading to tumor cure and formation of immunological memory.

MATERIALS & METHODS

Animals

University of Minnesota Institutional Animal Care and Use Committee approved all animal studies. We previously described *Kras*$^{LSL\text{-}G12D+}$, *Trp53*$^{LSL\text{-}R172H/+}$, *and p48*^{Cre} mice with >99.6% genetic similarity to C57BL/6J mice (16). We used 6–12-week-old female and male mice purchased from The Jackson Laboratory including C57BL/6J mice (000664) or mice backcrossed to C57BL/6 >10 generations including *Il27ra*$^{-/-}$ (018078), *Ifngr1*$^{-/-}$ mice (003288), and *Tnfrsf1a*$^{-/-}$ (003242). *Il10*^{eGFP} mice were generously provided by Dr. Sarah Hamilton and described (21, 22). *Il27p28*^{eGFP} mice were generated and provided by Dr. Ross Kedl (23).

Primary tumor epithelial cells

Autochthonous tumors from C57BL/6J *KPC* mice were cultured *in vitro* to generate primary PDA tumor epithelial cells as described (16, 20). The *KPC*2 and *KPC*2a CB-eGFP+ cells (20) were maintained below passage 15 in Basic Media (in 500 mL DMEM (Gibco) +10% FBS (Gibco) + 2.5 μg/ml Amphotericin B (Gibco) + 100 μg/ml pen/strep (Gibco) + 2.5 mg dextrose (Fisher Chemical) at 37°C and 5% CO_2. Media was sterile filtered and stored in the dark at 4°C.

Orthotopic tumor cell implantation

After reaching surgical plane anesthesia, a small incision was made in the right abdomen to access the pancreas. 1 ×10^5 tumor cells were injected into the pancreas in 20 μl of 60% matrigel (Discovery Labware) using an insulin syringe (Covidien) (20). Separate sets of sutures were used to close the peritoneum and skin (Ethicon). For the orthotopic tumor re-challenge experiments, a total of 1×10^5 CB+ *KPC*2a cells, or a 9:1 ratio of *KPC*2a:*KPC*2 (CB+:CB-) tumor cells, were implanted surgically into the pancreas in the same manner.

Production of $CB_{101–109}$:H-2D^b fluorescently labeled tetramer

H-2D^b-restricted biotinylated monomer was produced by incubating $CB_{101–109}$ peptide with purified H-2D^b and β2m followed by purification via Fast Protein Liquid Chromatography system (Aktaprime plus, GE health care) as we described (18). Biotinylated monomer was conjugated to streptavidin R-phycoerythrin or streptavidin BV421 (Invitrogen) to produce fluorescent $CB_{101–109}$:H-2D^b tetramer, which we validated previously (20).

In vivo monoclonal antibody treatments

On day 7 post orthotopic tumor implantation and following tumor establishment within the pancreas, 100 μg of agonistic αCD40 (FGK45, BioXcell) was diluted in sterile saline and injected intraperitoneally (i.p.). A separate cohort of tumor bearing mice received 200 μg of αPD-L1 (10F.9G2, BioXcell) i.p on days 7, 10 and 12 post orthotopic tumor implantation. Cohorts in Figure 1 received 200 μg αLag3 (clone C9B7W, BioXcell), αTim3 (RMT3–23, BioXcell) or αTIGIT (clone 1G9, BioXcell) alone, or in combination with αPD-L1 (10F.9G2) i.p. on days 7,10 and 12. Combination treated animals received both antibodies at the same timepoints. For *in vivo* antibody blockade of IL-27 or IL-10, 200 μg of αIL-27p28

(clone MM27.7B1, BioXcell) or αIL-10R (clone 1B1.3A, BioXcell) was diluted in sterile saline and injected i.p. on days 6, 10, 14, and 18 post orthotopic tumor implantation.

In vivo imaging

Abdominal hair was removed with Nair. High-resolution ultrasound imaging (Vevo 2100) was used to visualize a defined hypoechoic mass in the murine pancreas using abdominal landmarks (liver, portal vein, duodenum, spleen and kidneys) as described (16, 20). Tumor volume based on ultrasound measurements was calculated using a modified ellipsoidal formula: $Tumor\ volume = 1/2(length \times width^2)$. For bioluminescent imaging, tumor-bearing mice were injected with 100 μg of D-Luciferin (Promega) i.p. followed by image acquisition 11 minutes later using 0.5 second exposure time. Images were first acquired after 0.5 second exposure time with a binning of 8. When luminescence saturation occured, additional images with a binning of 2 and/or auto exposure setting were acquired. Tumor radiance was quantified in photons per second using IVIS 100 and Living Image software (Xenogen).

Preparation of mononuclear cells from tissues

Spleens were mechanically dissociated to single cells. Red blood cells (RBCs) were lysed by incubation in 1 mL of Tris-ammonium chloride (ACK) lysis buffer (GIBCO) for 1–2 minutes at room temperature in 15 mL conical tubes. 9 mL of T cell media (DMEM (GIBCO) + 10% FBS (GIBCO), 100 μg/ml pen/strep (GIBCO), 20 mM L-glutamine (GIBCO), 1x NEAA (GIBCO), and 50 μM β-mercaptoethanol (Sigma)) was added to quench lysis. Cells were spun at 1400 rpm for 5 minutes and stored in T cell media on ice until further analyses. Tumors were mechanically digested to single cells in a similar manner including 2 additional wash steps to remove cell debris and pancreatic enzymes.

Flow cytometry

T cells were stained with $CB_{101–109}$:H-2D^b-PE or -BV421 tetramer (1:100) in the presence of 1:500 Fc block (αCD16/32, Tonbo), and antibodies including murine CD45 (30F-11, Biolegend), CD8α (53–6.7, Tonbo), CD44 (IM7, BD), CD62L (MEL-14, Biolegend), Klrg1 (2F1, Biolegend), Cxcr3 (CXCR3–172, eBioscience), PD-1 (J43, Invitrogen), Tim-3 (RMT3–23, Biolegend), Lag-3 (C9B7W, Biolegend), Tigit (1G9, Biolegend), CD69 (H1.2F3, BD), CD103 (M290, BD), and/or CD49a (Ha31/8, BD) in the presence of live/dead stain (Tonbo Ghost dye in BV510 or APC ef780). For tetramer staining, we included a dump channel with antibodies to CD11b (M1/70, Tonbo) and CD19 (1D3, BD). Antibodies were diluted either 1:100 or 1:200 in FACs Buffer (PBS+2.5% FBS). Cells were fixed using Foxp3 transcription staining kit (Tonbo) for 30 minutes at 4°C, washed and intracellular stained with antibodies specific to Tox (TXRX, Invitrogen) and Granzyme B (NGZB, eBioscience). Intracellular staining was performed for 1 hour by diluting 1:100 in Fix/Perm buffer (Tonbo). For myeloid cells analysis, mononuclear cells were stained with 1:500 Fc blockade (αCD16/32, Tonbo) in combination with monoclonal antibodies specific to murine CD45 (30F11, Biolegend), CD19 (1D3, BD), NK1.1 (PK136, eBioscience), NKp46 (29A1.4, Biolegend), CD11b (M1/70, Tonbo), Ly6G (1A8, eBioscience), CD64 (X54–5/7.1. Biolegend), F4/80 (BM8, eBioscience), CD11c (N418, BD), I-A^b (M5/114 15.2, Invitrogen), CD8α (53–6.7, Tonbo), CD103 (M290, BD), Xcr1 (ZET, Biolegend), SIRPα (P84, Biolegend), PD-L1 (10F.9G2, Biolegend), Clec9a (7H11, Biolegend), CD40 (HM40–3,

Biolegend) and/or intracellular IRF8 (V3GYWCH, eBioscience) in the presence of live/dead stain (Tonbo Ghost dye in BV510 or APC ef780) for 30 minutes at 4ºC in the dark. Cells were fixed with 0.4% PFA for 15 minutes and cell counting beads (Thermo Fisher) were added to each sample prior to acquisition using a Fortessa 1770 flow cytometer and BD FACS Software. Data were analyzed using FlowJo software (version 10).

In vitro T cell culture

A total of 5×10^6 splenocytes from *Il10*^{eGFP} mice (21, 22) were cultured with anti-CD3 (1 μg/ml, clone 145–2c11 BD) + anti-CD28 (5 μg/ml, clone 37.51, BD) ± 50 ng/ml of recombinant murine IL-27 (R&D systems) in T cell media similar to as described (24). For the 7-day timepoint, IL-27 was replenished every 48 hours. Following either 2-day or 7-day stimulation, unfixed cells were stained with a live/dead cell stain (Tonbo Ghost dye), CD45 (30F-11, Biolegend), CD8α (53–6.7, Tonbo), CD4 (RM4–5, Tonbo), and Lag-3 (C9B7W, Biolegend) diluted 1:100 – 1:200 in FACs Buffer (PBS + 2.5% FBS) and analyzed for GFP expression by flow cytometry on the same day in triplicate. We stained additional samples with the identical above antibodies which then were fixed and permeabilized using the Foxp3 intracellular staining kit (Tonbo) followed by intracellular staining for Tox (TXRX, Invitrogen).

viSNE and FlowSOM Analysis

In Figure 1, samples were concatenated and CD8+tetramer+ T cells were analyzed using Flowjo version 10. The 6 clusters were identified in an unbiased manner using the FlowSOM algorithm plugin for Flowjo (25), where each cell of the 4 samples was assigned to one of 6 meta clusters based on expression of CTLA4, Tim3, Lag3, Tigit, IL-10, and PD1. ViSNE analysis was performed with default settings of 1000 iterations, 20 perplexity, 200 Eta, 0.5 Theta, and the channels CTLA4, Tim3, Lag3, Tigit, IL-10, PD1, and Sample ID were selected.

Intracellular cytokine staining and GFP quantification

To determine antigen-specific T cell cytokine production, single cell spleen and tumor suspensions were cultured ± $CB_{101–109}$ peptide (1 μg/ml Genscript) and Golgiplug (1:500 BD Biosciences) for 4–5 hours at 37°C incubator. Cells were subsequently stained with live/dead cell dye (Tonbo Ghost dye in BV510 or APC ef780) and antibodies including CD45 (30F-11, Biolegend), CD8α (53–6.7, Tonbo), CD44 (IM7, BD), and Klrg1 (2F1, Biolegend) diluted 1:200 in FACs Buffer (PBS+2.5% FBS) for 30 minutes in the dark at 4°C. Cells were fixed and permeabilized (BD Fixation Kit) and incubated with antibodies specific IFNγ (XMG1.2, Biolegend, 1:100) and TNFα (MP6-XT22, Biolegend, 1:100) diluted in permeabilization buffer overnight in the dark at 4°C. To calculate the proportion of GFP+ immune cells in *Il10*^{eGFP} and *Il27p28eGFP* tumor-bearing mice, we subtracted the mean background GFP+ signal identified in cell subsets isolated from spleen and tumor of non-reporter animals (n=3 mice per timepoint) from the GFP+ signal in cell subsets isolated from spleen and tumor of *Il10*^{eGFP} or *Il27*^{p28eGFP} animals (n=3–7 mice per timepoint) in Figures 2B, 2D, 2I, 2J and Supplemental Fig. 2G. Cells were collected using a Fortessa 1770 and Facs Diva software (BD Biosciences) and data was analyzed using FlowJo software (version 10).

Cell numbers normalized to tissue gram

Flow cytometry cell counting beads (Thermo Fisher) were added to each tube collected for flow cytometry. The number of live CD45+ cells collected per tube was determined using FlowJo analysis software and the equation: #CD45+ cells per tube (n) = (#Beads/#Cells) × (Concentration of beads × Volume of beads added). Total number of cells collected from the entire single cell suspension was determined by multiplying n by total number of stains. Cell numbers were normalized to gram of tissue by dividing cell numbers by gram (spleen or tumor).

Immunofluorescence

Tissues were embedded in OCT (Tissue-Tek) and stored at −80°C. 7 μm sections were cut using a Cryostat and fixed in acetone at −20°C for 10 minutes. Sections were rehydrated with PBS + 1% bovine serum albumin (BSA) and incubated for 1 hour at room temperature CD8-PE/Dazzle 594 (53–6.7, Biolegend, 1:100), panCK-FITC (Sigma-Aldrich, F3418, 1:200) and CD49a (Ha31/8, BD, 1:100) diluted in PBS + 1% BSA. Sections were washed 3X with PBS+1% BSA, 2X with PBS and mounted in DAPI Prolong Gold (Life Technologies). Images were acquired on a Leica DM6000 epifluorescent microscope at the University of Minnesota Center for Immunology using Imaris 9.1.0 (Bitplane).

TCGA database

PDA patient survival and gene expression data deposited in The Cancer Genome Atlas (TCGA) were analyzed using Gene Expression Profiling Interactive Analysis (GEPIA), http://gepia.cancer-pku.cn/.

Analysis of tumor escape variants

When tumor size was $>10^8$ radiance and/or >500 mm^3, tumors from 3 mice that escaped agonistic αCD40 (harvested at day 40–75), 2 tumors that escaped agonistic αCD40+αPD-L1 (harvested at day 80) ,and 2 tumors that escaped αPD-1+αPD-L1 (harvested at day 80) were expanded *in vitro* as described (20). Following *in vitro* establishment of cell lines (~1 week), 3×10^5 *KPC* tumor epithelial cells per well were plated in 6-well plates in tumor media. After 24 hours, supernatant was removed and replaced with tumor media ± 50 ng/ml recombinant mouse IFNγ (R&D Systems). After ~48 h, adherent tumor cells were lifted in 10 mM EDTA (Invitrogen), washed and stained with antibodies directly conjugated to PD-L1 (10F.9G2, BioLegend). Data were acquired on Fortessa flow cytometer (BD) using BD FACSDiva software and analyzed using FlowJo v10. Re-derived cell lines were also plated at equal numbers and cultured *in vitro* ± recombinant mouse IFNγ (100 ng/mL, R&D Systems) for 24 hours in 6-well plates. Cells were lifted in 10 mM EDTA (Invitrogen), RNA was extracted (QIAGEN RNeasy Mini Kit) and concentration/purity was assessed by Nanodrop. cDNA was generated using RT Buffer Mix and RT Enzyme Mix (Thermo Fisher). Real time PCR was performed in triplicate on a BioRad CFX96 Touch Real-Time PCR Detection System by measuring SYBR Green (BioRad) fluorescence for 40 cycles similar to as we described (20).

Statistical Analysis

Statistical analyses were performed using GraphPad software (version 7.0). All mouse experiments reflect n= 3–16 mice per group. Unpaired, two-tailed student's T test was used to compare 2-group data. One-way ANOVA and Tukey post-test were used for comparing >2-group data. Log-rank (Mantel-Cox) test was used to test for statistically significant differences in mouse survival. Data are presented as mean ± standard error of the mean (S.E.M.) and $p<0.05$ was considered significant. *, $p<0.05$; ** $p<0.005$; ***, $p<0.0005$.

RESULTS

Tumor-specific T cells progressively lose Granzyme B and IFNγ while increasing Tox and IL-10 in PDA

Tox is a transcription factor that can both promote pathogenic CD8 effector (T_{EFF}) T cells (26) and T_{EX} differentiation (27–30). We analyzed intratumoral $CB_{101–109}$:H-$2D^b$-specific T cells (Supplemental Fig. 1A) for intracellular expression of Tox and GzmB at various timepoints post orthotopic *KPC*2a (CB+) tumor implantation (Fig. 1A–B), a PDA mouse model we previously described (20). Compared to splenic tetramer+ T cells, Tox was elevated in intratumoral tetramer+ T cells 2-, 4- and 6-fold on days 7, 14 and 21, respectively (Fig. 1C). Tox levels were significantly increased in intratumoral T cells on day 14 as compared to day 7 and decreased by day 21 (Fig. 1C). GzmB levels were highest on day 7 and significantly decreased by day 14 in intratumoral tetramer+ T cells, (Fig. 1C–D). The proportion of Tox+Gzmb+ intratumoral tetramer+ T cells also progressively decreased (Fig. 1D). By day 21, most splenic tetramer+ T cells were Tox-Gzmb-, suggesting less antigenic stimulation (Fig. 1D). Despite tumor-specific T cell accumulation in PDA, T cell progressively were rendered defective in IFNγ production following peptide re-stimulation between days 7 and 14 (Fig. 1E and Supplemental Fig. 1B). In contrast, splenic tumor-specific T cells maintained IFNγ production following TCR signaling even on day 21 (Fig. 1E and Supplemental Fig. 1B). We observed a similar loss of TNFα production by intratumoral $CB_{101–109}$-specific T cells following *ex vivo* peptide re-stimulation (not shown and (20)). Intratumoral tetramer+ T cells produced more IL-10 than splenic tetramer+ T cells (Fig. 1F). Tetramer+ T cells tended to produce more IL-10 compared to tetramer- T cells, suggesting a dependency on chronic TCR signaling (Supplemental Fig. 1C). FlowSOM and viSNE clustering of tetramer+ T cells identified clusters 4 and 5 that were restricted to tumor and exhibited high expression of co-inhibitory receptors PD1, Lag3, and Tigit while such expression was absent in cluster 2 in spleen (Fig. 1G–I and Supplemental Fig. 1D). Moreover, cluster 5, which exhibited multiple coinhibitory receptor expression was also particularly elevated in IL-10 compared to cluster 4 (Fig. 1H–I). IL-10 was significantly increased in intratumoral tetramer+ T cells by day 14 post tumor implantation (Fig. 1J), a timepoint we have previously shown to render tumors refractory to monotherapy αPD-L1 (20). Thus, IL-10^{high} (cluster 5) vs. IL-10^{low} (cluster 4) T_{EX} may represent a continuum of T_{EX} formation. We next tested the functional significance of several coinhibitory receptors elevated in intratumoral T cells by administrating blocking antibodies starting on day 7 post tumor implantation. Lag3 blockade alone, or in combination with αPD-L1, significantly prolonged mouse survival and exhibited the strongest overall effect (Fig. 1K). However,

αLag3+αPD-L1 was not curative in most animals suggesting additional factors in the TME contribute to T_{EX} formation and tumor escape.

Agonistic αCD40 abrogates intratumoral myeloid cell production of IL-27 and T_{EX} formation

Due the enrichment of IL-10 in T_{EX}, we sought to identify a potential mechanism. IL-27 is a heterodimeric cytokine that is composed of IL-27p28 and Epstein-Barr virus-induced gene 3 (Ebi3), which is shared with IL-35 (31). IL-27 production by immunoregulatory dendritic cells (DCs) promotes the expansion of IL-10-producing CD4 T cells (32) and peripheral tolerance (33, 34). IL-27 also promotes CD8 T cell coinhibitory receptor expression (24) and is linked to T_{EX} program in melanoma (35). We identified high *IL27p28* significantly correlated with decreased overall survival in PDA patients (Fig. 2A). To first investigate the kinetics of *IL27p28* expression in PDA, we implanted *KPC*2a tumor cells into the pancreas of *Il27p28*^{GFP} reporter mice (23). *Il27p28*^{eGFP} was progressively increased in intratumoral CD45+ cells (Fig. 2B). In contrast, *Il27p28*^{eGFP} was not detected in healthy pancreas (Fig. 2C and Supplemental Fig. 2A). To further identify *Il27p28*^{eGFP}-expressing cell subsets, we used a gating strategy shown in Supplemental Fig. 2B. cDC1s express Xcr1 and are efficient at cross-presenting cell-associated antigen to prime naïve CD8+ T cells and cDC2s promote naïve CD4+ T cell priming (36–39). cDC1s co-expressed higher levels of IRF8 and CLEC9A as compared to cDC2s (Supplemental Fig. 2C), validating our gating strategy. Il27p28 by granulocytes increased earliest following tumor implantation (day 7), followed by cDC2s, TAMs, cDC1s (day 14), and B cells (day 21) (Fig. 2D). Tumor growth was delayed in *Il27ra*$^{-/-}$ mice (Fig. 2E and Supplemental Fig. 2D) despite similar tumor-specific T cell frequency (Fig. 2F) and number (not shown). A significantly lower proportion of intratumoral tumor-specific T cells expressed Tox in *Il27ra*$^{-/-}$ mice (Fig. 2G–H), suggesting IL-27 may promote tumor growth via inducing T_{EX}. This effect was independent of tumor size because Tox was increased in tetramer+ T cells at day 21 in *Il27ra*$^{-/-}$ mice compared to tetramer+ T cells isolated on day 14 from wild type animals, timepoints when tumor size is similar between these cohorts (Fig. 2E). As depleting a cytokine for therapeutic purposes would require prolonged dosing, we began to test clinically applicable TME-modulating approaches that may reprogram or change IL-27 producing myeloid cells in PDA. Agonistic αCD40 significantly decreased *Il27p28* production by intratumoral CD45+ cells, including granulocytes, TAMs and cDC2s (Fig. 2I and Supplemental Fig. 2E). As IL-10 can be induced by IL-27 signaling in CD4+ T cells (32), we next analyzed how agonistic αCD40 impacted IL-10 by utilizing the *Il10*^{egfp} reporter mice. Agonistic αCD40 significantly decreased IL-10 production by total intratumoral CD45+ cells with a significant decrease in IL-10 by TAMs (Supplemental Fig. 2F–G). Agonistic αCD40 significantly decreased intratumoral CD8+ T cell IL-10 production (Fig. 2J). In contrast, αPD-L1 had no effect on immune cell expression of these cytokines (Fig. 2I–J and Supplemental Fig. 2E–G). The decrease in IL-10 production following agonistic αCD40 correlated with a concomitant increase in Granzyme B in intratumoral tetramer+ T cells (Fig. 2K). To investigate if IL-10 or IL-27 impacted tumor growth, we blocked either IL-10R or IL-27p28 as shown in Supplemental Fig. 2H. Blocking either IL-10R or IL-27p28 significantly decreased tumor size (Fig. 2L).

The above data suggest that agonistic αCD40 may be altering IL-10 production in T cells by decreasing IL-27 in myeloid cells. We therefore next tested if IL-27 directly enhanced IL-10 production in CD4 and CD8 T cells *in vitro*. IL-27 significantly increased IL-10 production by CD8+ T cells on days 2 and 7, and by CD4+ T cells on day 2 post T cell activation (Fig. 2M–2N). Further, IL-27 increased the amount of IL-10 produced by CD8+ T cells and CD4+ T cells (Fig. 2O). However, IL-27 did not impact TOX or Lag3 expression in the *in vitro* activated T cells (Fig 2P). While further studies are necessary, the results are consistent with agonistic αCD40 mitigating IL-10 production by CD8+ T cells via downmodulation of IL-27.

Agonistic αCD40 and αPD-L1 blockade therapy promote pancreatic cancer eradication

Because CD40 agonist decreased IL-27 by intratumoral myeloid cells, we next tested if agonistic αCD40 enhanced immune checkpoint blockade using αPD-L1. After tumor establishment, mice were randomly enrolled to receive αCD40, αPD-L1, or the combination (Fig. 3A). Tumors relapsed following either monotherapy yet were undetectable following αCD40+αPD-L1 (Fig. 3B–C). The combination significantly prolonged animal survival resulting in cures in 63% (10/16) animals (Fig. 3D). Therefore, we next investigated the individual contribution of these therapies on tumor-specific T cells by first measuring cytokine-producing tumor-specific T cells at 1-week post therapy, a timepoint at which tumor size is equivalent and thus would not be a contributing variable to T cell phenotype or function (Fig. 3E). We found agonistic αCD40 alone failed to increase the number of IFNγ-producing tumor-specific CD8+ T cells in spleen or tumor (Fig. 3F). In contrast, combination therapy significantly increased the number of intratumoral T cells producing IFNγ or co-producing IFNγ and TNFα (Fig. 3F). αPD-L1 monotherapy or αCD40+αPD-L1 increased splenic CB-specific T cell number on day 14 (Fig. 3G), consistent with enhanced peripheral T cell priming, survival, and/or proliferation post-αPD-L1 treatment similar to our prior study (20). αCD40+αPD-L1 also increased intratumoral CB-specific T cell number (Fig. 3G). Similar to cytokine results, agonistic αCD40 failed to increase the number of tumor-specific T cells in spleen and tumor. These results are consistent with a failure of agonist αCD40 alone to prime T cells in a vaccination setting (40). While the frequency of tetramer+ T cells increased in the spleen post agonistic αCD40+αPD-L1 on day 14 (Supplemental Fig. 3A), it was unchanged in the tumor, potentially reflecting an influx of additional T cell antigen specificities and consistent with an increase in total intratumoral CD8+ T cells (Supplemental Fig. 3B). Intratumoral $CB_{101–109}$:H-$2D^b$-specific T cells contracted >5 fold between days 14 and 21 following αCD40+αPD-L1 (Fig. 3G), coinciding with tumor clearance.

Klrg1 is expressed on effector T cells during acute viral infection (41, 42), on both short-lived (43) or long-lived effector cells (44), and is downregulated during memory transition (45). Our prior study showed that Klrg1 and Lag3 could distinguish functional effector from exhausted T cells in PDA, with Klrg1+Lag3- tumor-specific T cells correlating with tumor control (20). There is an inverse relationship between Tox and Klrg1 expression in CD8 T cells during viral infection (29, 30). Both αCD40 monotherapy and αCD40+αPD-L1 increased the proportion of intratumoral Klrg1+tetramer+ T cells on day 14 (Fig. 3H). By

day 21, however, Klrg1+ tetramer+ T cells markedly decreased following αCD40 (Fig. 3H), suggesting αCD40 may promote short-lived effector T cells at the expense of T_{EX}.

We previously showed that endogenous intratumoral tumor-specific T cells upregulate PD-1, Lag-3, TIGIT, and Tim-3 and are rapidly rendered exhausted (20). Therefore, we next assessed if inhibitory receptor expression and Tox were impacted by these immunotherapies. Tox was increased in tumor-specific T cells in the tumor vs. spleen (Fig. 3I–3J), consistent with chronic antigen stimulation. αCD40 and αCD40+αPD-L1 significantly decreased Tox + tetramer+ T cells in PDA (Fig. 3I). αCD40 or αCD40+αPD-L1 significantly decreased the proportion of intratumoral CB-specific T cells that co-expressed multiple inhibitory receptors (Supplemental Fig. 3C). Tox was also decreased in intratumoral non-tetramer-binding CD8+ T cells following combination therapy (Supplemental Fig. 3D). αCD40+αPD-L1 significantly decreased tumor weight in the rapidly growing orthotopic parental CB- *KPC* model (Supplemental Fig. 3E). However, we did not observe tumor regressions in this model suggesting that the therapeutic effects of this combination require the presence of neoantigen-specific T cells. Future studies that incorporate chemotherapy may help activate endogenous tumor-reactive T cells in tumors with lower antigenicity (12).

αCD40+αPD-L1 promotes long-lived effector and resident memory T cells capable of tumor rejection

Tissue resident memory T cells (T_{RM}) gene signatures correlate with improved outcomes in breast, skin, and lung cancer (46–48). While well-studied in mucosa, T_{RM} formation in pancreas is less clear. Therefore, we tested if tetramer+ T cells persisted long-term in cured immunotherapy-treated mice and if they exhibited phenotypic traits of T_{RM}. 12–15% of CD8+ T cells were tetramer+ in pancreas as well as sites for PDA metastasis including liver and lung (Fig. 4A). Numerically, most tetramer+ T cells resided in the spleen, however (Fig. 4B). Pancreas-residing tetramer+ T cells were enriched for T_{RM} markers CD49a and CD103 (Fig. 4C–D) yet lacked CD69 (Supplemental Fig. 4A), perhaps reflecting tissue-dependent variability of CD69 on T_{RM} (49). Tetramer+ cells expressed higher PD-1 and Lag-3 in pancreas compared to spleen (Fig. 4D and Supplemental Fig. 4B), which may be due to epigenetic modification of the PD-1 locus (50). CD49a and CD103 MFI was highest in pancreas tetramer+ T cells (Supplemental Fig. 4C), potentially due to differences in surrounding tissue or prior antigen encounter. Rare CD8+CD49a+ T cells were detected in close contact with CD49+ stromal cells in pancreas from cured mice yet not in control pancreas or tumor (Supplemental Fig. 4D). To test if memory T cells could reject tumors, we re-challenged a separate cohort of cured mice on day 100, which rapidly rejected CB+ tumors (Fig. 4E–F, and Supplemental Fig. 4E–F). Further, 66% (2/3) mice rejected a 9:1 ratio of CB+:CB- tumor re-challenge (Fig. 4E–F and Supplemental Fig. 4E–F), consistent with engaging tumor-reactive memory of T cells specific to native tumor antigens. On day 30 post challenge, pancreas weight was normal in the 5/6 animals with no *in vivo* tumor growth (Supplemental Fig. 4G) and we readily detected tetramer+ T cells in pancreas from recipients (Supplemental Fig. S4H–I). Tetramer+ T cell number increased 10-fold in circulation and 100-fold within the pancreas compared to control cured mice (Fig. 4G). The contribution of systemic vs. resident memory T cells to the overall anti-tumor effect is warranted in future studies.

Abrogating Tnfrsf1a in non-tumor/host cells overcomes immune escape following αCD40+αPD-L1 therapy

To investigate how tumors escaped αCD40+αPD-L1 in the fraction of animals, we re-derived tumor escape variants (EVs) from mice treated with αCD40 (n=3) or αCD40+αPD-L1 (n=2). Compared to tumor cells prior to implantation, EVs expressed lower CB-eGFP, and one lost CB-eGFP entirely (Fig. 4H and Supplemental Fig. 4J). Similar to our prior study targeting the PD1 pathway (20), EVs were defective in *Tap1* induction following culture with IFNγ (Fig. 4I) resulting in low cell surface MHC class I (not shown), while retaining IFNγ-induced PD-L1 (Supplemental Fig. 4J).

We hypothesized that the functional loss of IFNγ and TNFα production by T_{EX} in PDA may contribute to tumor escape following αCD40+αPD-L1. To begin to test this hypothesis, we orthotopically implanted *KPC*2a tumors into mice that lacked *Ifngr1* or *Tnfrsf1a* only on host cells and treated animals at day 7 ± αCD40+αPD-L1 as shown in Figure 3. *Ifngr1*$^{-/-}$ recipients failed to eradicate tumors following αCD40+αPD-L1 (Fig. 4J–K), demonstrating a critical role for IFNγ signaling on non-tumor/host cells for antitumor activity. In contrast, tumor growth was mitigated in untreated *Tnfrsf1a*$^{-/-}$ mice and remarkably, αCD40+αPD-L1 led to tumor eradication in all *Tnfrsf1a*$^{-/-}$ mice (Fig. 4J–L). While both wild type (WT) and *Tnfrsf1a*$^{-/-}$ mice generated numerically similar long-lived memory tetramer+ T cells in blood following αCD40+αPD-L1 and cure (not shown), most circulating tetramer+ T cells were CD44+CD62L- and positive for Cxcr3 or Klrg1 consistent with a long-lived effector memory phenotype rather than central memory (Fig. 4M). In cured *Tnfrsf1a*$^{-/-}$ mice, a higher proportion of circulating tetramer+ T cells were CD44+CD62L+, consistent with a central memory phenotype (Fig. 4M). Tumors did not recur in 100% of *Tnfrsf1a*$^{-/-}$ mice following αCD40+αPD-L1 resulting in prolonged survival compared to untreated *Tnfrsf1a*$^{-/-}$ mice (Fig. 4N). Thus, TNFα signaling on host cells can promote pancreatic cancer escape during immunotherapy.

DISCUSSION

Immune checkpoint blockade is transforming the standard of care for many advanced malignancies. However, PDA is largely resistant to PD-1 and CTLA-4 inhibition (7). We previously showed that αPD-L1 fails to reinvigorate intratumoral T_{EX}. Instead, αPD-L1 expands peripheral tumor-specific T cells required for transient antitumor effects (20). PD-1 blockade induces clonal replacement of T cells in human skin carcinoma (51), consistent with expanding peripheral T cells. As PD-1 is induced following TCR signaling, we posit that PD-1 may suppress high affinity tumor-specific T cells that are a target for PD-1/PD-L1 blockade. Based on our results that a combination of PD-L1 blockade, agonistic αCD40 and interfering with Tnfα signaling results in cures in 100% of PDA-bearing animals, we hypothesize that there are three requirements for PDA eradication: 1) expansion of functional high-affinity tumor-antigen specific T cell clone(s), 2) abrogating suppressive intratumoral myeloid cell function, and 3) interfering with chronic inflammatory signaling induced by TNFα. Thus, our study provides a framework to inform the development of effective immunotherapy combinations, including T cell engineering strategies for patient treatment (16, 52).

While PDA-specific CD8+ T cells lose critical effector functions in the TME, we show that they retain and/or acquire new potentially regulatory functions including IL-10. As IL-10 is a suppressive cytokine, autocrine IL-10 may undermine T cell antitumor activity. We demonstrate IL-27 increases IL-10 in activated CD8+ and CD4+ T cells in vitro, consistent with a prior study that IL-27 induces IL-10 in CD4+ T cells (32). However, IL-27 did not increase TOX or Lag3 expression by *in vitro* activated T cells suggesting that the effects of agonistic αCD40 on these T cell markers may extend beyond IL-27 *in vivo*. However, the in vitro studies did not include chronic TCR signaling. Further investigation into the role autocrine IL-10 during T_{EX} differentiation during chronic antigen encounter is of interest.

PD-L1 blockade did not alter intratumoral myeloid cell IL-27p28 and intratumoral CD8+ T cell IL-10 production. In contrast agonistic αCD40 significantly decreased both IL-27p28 in myeloid cells and IL-10 in CD8+ T cells. Further investigation will be required to identify how agonistic αCD40 interferes with intratumoral myeloid cell production of IL-27. Possibilities include expanding a new wave of myeloid precursors, reprogramming intratumoral myeloid cells, or indirectly by induction of functional intratumoral antigen-specific T cells. Paradoxically, when used in a vaccination setting, agonistic αCD40 combined with a TLR agonist promotes T cell priming via IL-27 production by cDC1s (23, 53). The identical IL-27p28 reporter strain (23) was used in these two distinct biological contexts. In a tumor setting, multiple intratumoral myeloid subsets express IL-27, which is progressively increased during tumor growth and may be dependent on antigen-specific T cells that are chronically activated. Abrogating IL-27 in DCs sustains IFNγ production by CD4+ T cells, exacerbating hepatitis in a mouse model (54). IL-27 signaling in DCs can induce peripheral T cell tolerance, mitigate autoimmunity (33, 34) and promote inhibitory receptor expression on T cells (24, 35). *IL27* polymorphisms are observed in patients with chronic inflammatory diseases (55, 56). Finally, as high *IL27P28* significantly correlates with decreased overall survival in PDA patients (Fig. 2A), our study supports a predominantly regulatory role for IL-27 in PDA.

Either abrogating IL-27 or administration of agonistic αCD40 significantly reduced the proportion of intratumoral tumor-specific T cells that expressed Tox, which is required for T_{EX} survival during chronic antigen stimulation (27–30). Tox appears insufficient to identify T_{EX}, however, as it is also expressed in functional T_{EFF} early after tumor implantation (Fig. 1) and after in vitro activation (Fig. 2). The role of Tox appears context dependent as it was required to drive highly functional and pathogenic T cells in the central nervous system (26).

Although agonistic αCD40 likely has additional anti-tumor affects, our results suggest agonistic αCD40 may operate by decreasing myeloid cell IL-27 production resulting in switching intratumoral T cell fate from the Tox+ T_{EX} lineage toward to short-lived Klrg1+ effector T cells. As agonistic αCD40 alone is insufficient for cure, the expansion of either qualitatively and/or quantitatively new T cell clones in the periphery following αPD-L1, potentially expanding higher affinity T cell clones, is operating in a non-redundant manner from agonistic αCD40 and is necessary for cure. We find no evidence that agonistic αCD40 alone promotes T cell priming to a tumor-specific antigen, consistent with prior studies in a vaccination setting where agonistic αCD40 without TLR signaling poorly primed antigen-specific CD8+ T cells (40). Instead, we find agonistic αCD40 alters the TME and

intratumoral T cell differentiation. Our favored hypothesis is that agonistic αCD40 alters the cross-talk between tumor-specific T cells and myeloid cells within the TME, thereby overriding the contribution of chronic TCR signaling toward T_{EX} and instead instructing T cell fate toward cytotoxic effector T cells. Alternatively, agonistic αCD40 may instead qualitatively alter the program of T cell differentiation in the periphery.

Functional IL-27 is produced by activated antigen-presenting cells and is comprised of two subunits, Ebi3 and IL-27p28 (31). Reporter mice demonstrate enhanced IL-27p28 expression within 6 hours following vaccination (23). Expression of both Ebi3 (57) and IL-27p28 (58) are upregulated following CD40 signaling. In addition, signaling through TLR3, 4, or 9 also promote IL-27p28 expression (59). IL-27p28 can be secreted independently of Ebi3 and in this form is known as IL-30. IL-30 is produced by prostate cancer stem cells and drives immunotherapy resistance and metastasis (60), raising the possibility that IL-27p28 blockade may have had IL-27R independent effects. Nonetheless, in our system *Il27ra*$^{-/-}$ mice had impaired tumor growth and fewer Tox+ T cells suggesting IL-27 signaling promotes T_{EX}. In addition, Ebi3 can pair with IL12p30 to generate IL-35 which is secreted by T cells and B cells (61). Intratumoral B cells secrete IL-35 which suppresses CD8 T cell expression of CXCR3, CCL5, and IFNγ through STAT3 signaling (62). Thus, additional cytokines in the TME related to IL-27 may participated in immune suppression. Notably, IL-35 promotes T cell exhaustion whereas IL-27R signaling had no significant effect on tumor growth in a subcutaneous B16 melanoma model (63), suggesting a TME-role for these cytokines. Understanding the hierarchy is the challenge ahead and may depend upon the extent that a tumor-specific T cell response is engaged.

T_{RM} development in many tissues is well-characterized (49, 64, 65). Improved outcomes are associated with a T_{RM} signature in some human malignancies (46–48). However, the factors that govern pancreas T_{RM} differentiation and maintenance are unclear, especially in the context of cancer immunotherapy. We show that PD-1 remains elevated on pancreas-residing memory tumor-antigen specific T cells following αCD40+αPD-L1 treatment and cure, despite no evidence for remaining tumor. Tumor-specific T cells in the pancreas also acquired a T_{RM} phenotype including expression of CD44, PD-1, CD49a and CD103. The PD-1 locus can become epigenetically fixed in T cells (50), which may explain our observation of PD-1 retention in pancreas T_{RM}. Since αCD40+αPD-L1 promoted a T_{RM} phenotype to a greater extent in the pancreas compared to the lung and liver, such differences may be indicative of the characteristics of the surrounding tissue or dependent on if T cells experienced antigen at that site. In the pancreas, T_{RM}-like tetramer+ T cells appear to associate with CD49a+ stromal cells, which is expressed by mesenchymal stem cells that express pro-survival and anti-inflammatory factors (66). Notably, αCD40+αPD-L1-treated mice not only cured tumor but rendered mice resistant to orthotopic tumor re-challenge with neoantigen+ PDA as well as in a mixed tumor cell setting in which a fraction of tumor cells did not express the target neoantigen. The contribution of CD4+ vs. CD8+ memory T cells reactive to native PDA antigens to the overall antitumor effect remains to be identified.

A striking and unexpected result from our study is the regulatory role of Tnfr1 signaling on non-tumor/host cells during pancreatic cancer immunotherapy. Previously, we thought that the loss of TNFα production in both endogenous and engineered intratumoral exhausted

CD8+ T cells (16, 20) was a detriment to antitumor immunity. There are additional sources of TNFα in PDA, however, including TAMs which are abundant in PDA (67). *Tnfrsf1a*$^{-/-}$ mice have increased susceptibility to intracellular pathogens demonstrating Tnfr1 signaling is critical for some TNFα pro-inflammatory function (68). However, chronic inflammation may not be beneficial to tumor immunity (69). Contrasting with our study, TNFα was critical for establishing tumor-immune equilibrium in a melanoma model (70). However, prior studies in PDA models show both tumor-promoting and anti-tumor effects of TNFα (71) and its blockade can enhance chemotherapy efficacy by reducing tumor desmoplasia (72). Tnfr1 signaling on bone-marrow derived cells also promotes gastric tumor progression (73). TNFα blockade uncouples toxic autoimmune colitis from efficacy of PD-1+CTLA4 blockade and increases efficacy in a colorectal cancer mouse model (74). During chronic viral infection, chronic TNFα promotes PD-1 on T cells and perturbing Tnfr1 restores antiviral immunity through relieving persistent NFκB signaling (75). Thus, the role for TNFα in cancer immunity is context dependent and further investigation of the relevant source and target cell for interfering with immunotherapy in PDA is of particular interest. There are numerous TNFα inhibitors clinically approved and some initially tested in the clinic and can interfere with immune-related adverse events (irAEs) following immune checkpoint blockade in cancer patients (76). Together, our study supports the further investigation into how to combine TNFα inhibitors to promote immunotherapy efficacy.

Although still ongoing, interim analysis of an early phase clinical trial of a CD40 agonist, gemcitabine + nab-paclitaxel with or without a PD-1 inhibitor has therapeutic benefit in newly diagnosed metastatic pancreatic cancer (17). The promising clinical results support the validity of our animal model that permits interrogating PDA-specific T cells and highlight the possibility that a substantial fraction of human PDAs contain endogenous tumor-reactive T cells despite a relatively low mutational burden.

Supplementary Material

Refer to Web version on PubMed Central for supplementary material.

ACKNOWLEDGEMENTS

We acknowledge University of Minnesota Imaging Core for assistance with IVIS imaging and quantification. We acknowledge the University of Minnesota Flow Cytometry Resource for technical assistance. We thank Dr. Sarah Hamilton for providing the *Il10*^{eGFP} reporter mice. We thank Anna Panek for helpful feedback on the manuscript. We thank colleagues at the Center for Immunology at the U of M for helpful discussions.

FUNDING

A.L.B. is supported by a computational training award from the American Association of Immunologists. M.R.R. is supported by NIH T32 AI007313. E.J.S. and T.D.M. are supported by NIH T35 AI118620. I.M.S. is supported by an AACR Pancreatic Cancer Action Network Career Development Award (17–20-25-STRO), AACR Pancreatic Cancer Action Network Catalyst Award (19–35-STRO), an American Cancer Society Institutional Research Grant (124166-IRG-58–001-55-IRG65) and pilot awards from the Masonic Cancer Center and Cancer Research Training Initiative (University of Minnesota Medical School).

REFERENCES

1. Siegel RL, Miller KD, and Jemal A. 2018. Cancer statistics, 2018. CA. Cancer J. Clin.

2. Von Hoff DD, Ramanathan RK, Borad MJ, Laheru DA, Smith LS, Wood TE, Korn RL, Desai N, Trieu V, Iglesias JL, Zhang H, Soon-Shiong P, Shi T, Rajeshkumar NV, Maitra A, and Hidalgo M. 2011. Gemcitabine plus nab-paclitaxel is an active regimen in patients with advanced pancreatic cancer: A phase I/II trial. J. Clin. Oncol.

3. Vogl UM, Andalibi H, Klaus A, Vormittag L, Schima W, Heinrich B, Kafka A, Winkler T, and Öhler L. 2019. Nab-paclitaxel and gemcitabine or FOLFIRINOX as first-line treatment in patients with unresectable adenocarcinoma of the pancreas: Does sequence matter? 11 Medical and Health Sciences 1112 Oncology and Carcinogenesis. BMC Cancer.

4. Hu-Lieskovan S, and Ribas A. 2017. New Combination Strategies Using Programmed Cell Death 1/ Programmed Cell Death Ligand 1 Checkpoint Inhibitors as a Backbone. Cancer J. (United States)

5. Hu ZI, Shia J, Stadler ZK, Varghese AM, Capanu M, Salo-Mullen E, Lowery MA, Diaz LA, Mandelker D, Yu KH, Zervoudakis A, Kelsen DP, Iacobuzio-Donahue CA, Klimstra DS, Saltz LB, Sahin IH, and O'Reilly EM. 2018. Evaluating mismatch repair deficiency in pancreatic adenocarcinoma: Challenges and recommendations. Clin. Cancer Res.

6. Hu ZI, Hellmann MD, Wolchok JD, Vyas M, Shia J, Stadler ZK, Diaz LA, and O'Reilly EM. 2018. Acquired resistance to immunotherapy in MMR-D pancreatic cancer. J. Immunother. Cancer

7. O'Reilly EM, Oh DY, Dhani N, Renouf DJ, Lee MA, Sun W, Fisher G, Hezel A, Chang SC, Vlahovic G, Takahashi O, Yang Y, Fitts D, and Philip PA. 2019. Durvalumab with or Without Tremelimumab for Patients with Metastatic Pancreatic Ductal Adenocarcinoma: A Phase 2 Randomized Clinical Trial. JAMA Oncol.

8. Steele CW, Karim SA, Leach JDG, Bailey P, Upstill-Goddard R, Rishi L, Foth M, Bryson S, McDaid K, Wilson Z, Eberlein C, Candido JB, Clarke M, Nixon C, Connelly J, Jamieson N, Carter CR, Balkwill F, Chang DK, Evans TRJ, Strathdee D, Biankin AV, Nibbs RJB, Barry ST, Sansom OJ, and Morton JP. 2016. CXCR2 Inhibition Profoundly Suppresses Metastases and Augments Immunotherapy in Pancreatic Ductal Adenocarcinoma. Cancer Cell.

9. Jiang H, Hegde S, Knolhoff BL, Zhu Y, Herndon JM, Meyer MA, Nywening TM, Hawkins WG, Shapiro IM, Weaver DT, Pachter JA, Wang-Gillam A, and DeNardo DG. 2016. Targeting focal adhesion kinase renders pancreatic cancers responsive to checkpoint immunotherapy. Nat. Med.

10. Kaneda MM, Messer KS, Ralainirina N, Li H, Leem CJ, Gorjestani S, Woo G, Nguyen AV, Figueiredo CC, Foubert P, Schmid MC, Pink M, Winkler DG, Rausch M, Palombella VJ, Kutok J, McGovern K, Frazer KA, Wu X, Karin M, Sasik R, Cohen EEW, and Varner JA. 2016. PI3Kγ 3 is a molecular switch that controls immune suppression. Nature.

11. Beatty GL, Chiorean EG, Fishman MP, Saboury B, Teitelbaum UR, Sun W, Huhn RD, Song W, Li D, Sharp LL, Torigian DA, O'Dwyer PJ, and Vonderheide RH. 2011. CD40 agonists alter tumor stroma and show efficacy against pancreatic carcinoma in mice and humans. Science (80-.).

12. Winograd R, Byrne KT, Evans RA, Odorizzi PM, Meyer ARL, Bajor DL, Clendenin C, Stanger BZ, Furth EE, Wherry EJ, and Vonderheide RH. 2015. Induction of T-cell immunity overcomes complete resistance to PD-1 and CTLA-4 blockade and improves survival in pancreatic carcinoma. Cancer Immunol. Res.

13. Luheshi NM, Coates-Ulrichsen J, Harper J, Mullins S, Sulikowski MG, Martin P, Brown L, Lewis A, Davies G, Morrow M, and Wilkinson RW. 2016. Transformation of the tumour microenvironment by a CD40 agonist antibody correlates with improved responses to PD-L1 blockade in a mouse orthotopic pancreatic tumour model. Oncotarget.

14. Ma HS, Poudel B, Torres ER, Sidhom JW, Robinson TM, Christmas B, Scott B, Cruz K, Woolman S, Wall VZ, Armstrong T, and Jaffee EM. 2019. A CD40 Agonist and PD-1 Antagonist Antibody Reprogram the Microenvironment of Nonimmunogenic Tumors to Allow T-cell–Mediated Anticancer Activity. Cancer Immunol. Res.

15. Morrison AH, Diamond MS, Hay CA, Byrne KT, and Vonderheide RH. 2020. Sufficiency of CD40 activation and immune checkpoint blockade for T cell priming and tumor immunity. Proc. Natl. Acad. Sci. U. S. A.

16. Stromnes IM, Schmitt TM, Hulbert A, Brockenbrough JS, Nguyen HN, Cuevas C, Dotson AM, Tan X, Hotes JL, Greenberg PD, and Hingorani SR. 2015. T Cells Engineered against a Native Antigen Can Surmount Immunologic and Physical Barriers to Treat Pancreatic Ductal Adenocarcinoma. Cancer Cell 28.

17. Vonderheide RH 2020. CD40 Agonist Antibodies in Cancer Immunotherapy. Annu. Rev. Med. 71: 47–58. [PubMed: 31412220]

18. Stromnes IM, Burrack AL, Hulbert A, Bonson P, Black C, Brockenbrough JS, Raynor JF, Spartz EJ, Pierce RH, Greenberg PD, and Hingorani SR. 2019. Differential effects of depleting versus programming tumor-associated macrophages on engineered T cells in pancreatic ductal adenocarcinoma. Cancer Immunol. Res. 7.

19. Evans RA, Diamond MS, Rech AJ, Chao T, Richardson MW, Lin JH, Bajor DL, Byrne KT, Stanger BZ, Riley JL, Markosyan N, Winograd R, and Vonderheide RH. 2016. Lack of immunoediting in murine pancreatic cancer reversed with neoantigen. JCI Insight.

20. Burrack AL, Spartz EJ, Raynor JF, Wang I, Olson M, and Stromnes IM. 2019. Combination PD-1 and PD-L1 Blockade Promotes Durable Neoantigen-Specific T Cell-Mediated Immunity in Pancreatic Ductal Adenocarcinoma. Cell Rep. 28.

21. Kamanaka M, Huber S, Zenewicz LA, Gagliani N, Rathinam C, O'Connor W, Wan YY, Nakae S, Iwakura Y, Hao L, and Flavell RA. 2011. Memory/effector (CD45RBlo) CD4 T cells are controlled directly by IL-10 and cause IL-22-dependent intestinal pathology. J. Exp. Med.

22. Burrack KS, Huggins MA, Taras E, Dougherty P, Henzler CM, Yang R, Alter S, Jeng EK, Wong HC, Felices M, Cichocki F, Miller JS, Hart GT, Johnson AJ, Jameson SC, and Hamilton SE. 2018. Interleukin-15 Complex Treatment Protects Mice from Cerebral Malaria by Inducing Interleukin-10-Producing Natural Killer Cells. Immunity.

23. Kilgore AM, Welsh S, Cheney EE, Chitrakar A, Blain TJ, Kedl BJ, Hunter CA, Pennock ND, and Kedl RM. 2018. IL-27p28 Production by XCR1 + Dendritic Cells and Monocytes Effectively Predicts Adjuvant-Elicited CD8 + T Cell Responses. ImmunoHorizons.

24. DeLong JH, O'Hara Hall A, Rausch M, Moodley D, Perry J, Park J, Phan AT, Beiting DP, Kedl RM, Hill JA, and Hunter CA. 2019. IL-27 and TCR Stimulation Promote T Cell Expression of Multiple Inhibitory Receptors. ImmunoHorizons.

25. Van Gassen S, Callebaut B, Van Helden MJ, Lambrecht BN, Demeester P, Dhaene T, and Saeys Y. 2015. FlowSOM: Using self-organizing maps for visualization and interpretation of cytometry data. Cytom. Part A.

26. Page N, Klimek B, De Roo M, Steinbach K, Soldati H, Lemeille S, Wagner I, Kreutzfeldt M, Di Liberto G, Vincenti I, Lingner T, Salinas G, Brück W, Simons M, Murr R, Kaye J, Zehn D, Pinschewer DD, and Merkler D. 2018. Expression of the DNA-Binding Factor TOX Promotes the Encephalitogenic Potential of Microbe-Induced Autoreactive CD8+ T Cells. Immunity.

27. Alfei F, Kanev K, Hofmann M, Wu M, Ghoneim HE, Roelli P, Utzschneider DT, von Hoesslin M, Cullen JG, Fan Y, Eisenberg V, Wohlleber D, Steiger K, Merkler D, Delorenzi M, Knolle PA, Cohen CJ, Thimme R, Youngblood B, and Zehn D. 2019. TOX reinforces the phenotype and longevity of exhausted T cells in chronic viral infection. Nature.

28. Scott AC, Dündar F, Zumbo P, Chandran SS, Klebanoff CA, Shakiba M, Trivedi P, Menocal L, Appleby H, Camara S, Zamarin D, Walther T, Snyder A, Femia MR, Comen EA, Wen HY, Hellmann MD, Anandasabapathy N, Liu Y, Altorki NK, Lauer P, Levy O, Glickman MS, Kaye J, Betel D, Philip M, and Schietinger A. 2019. TOX is a critical regulator of tumour-specific T cell differentiation. Nature.

29. Khan O, Giles JR, McDonald S, Manne S, Ngiow SF, Patel KP, Werner MT, Huang AC, Alexander KA, Wu JE, Attanasio J, Yan P, George SM, Bengsch B, Staupe RP, Donahue G, Xu W, Amaravadi RK, Xu X, Karakousis GC, Mitchell TC, Schuchter LM, Kaye J, Berger SL, and Wherry EJ. 2019. TOX transcriptionally and epigenetically programs CD8+ T cell exhaustion. Nature.

30. Yao C, Sun HW, Lacey NE, Ji Y, Moseman EA, Shih HY, Heuston EF, Kirby M, Anderson S, Cheng J, Khan O, Handon R, Reilley J, Fioravanti J, Hu J, Gossa S, Wherry EJ, Gattinoni L, McGavern DB, O'Shea JJ, Schwartzberg PL, and Wu T. 2019. Single-cell RNA-seq reveals TOX as a key regulator of CD8+ T cell persistence in chronic infection. Nat. Immunol.

31. Pflanz S, Timans JC, Cheung J, Rosales R, Kanzler H, Gilbert J, Hibbert L, Churakova T, Travis M, Vaisberg E, Blumenschein WM, Mattson JD, Wagner JL, To W, Zurawski S, McClanahan TK, Gorman DM, Bazan JF, De Waal Malefyt R, Rennick D, and Kastelein RA. 2002. IL-27, a heterodimeric cytokine composed of EBI3 and p28 protein, induces proliferation of naive CD4+T cells. Immunity.

32. Ilarregui JM, Croci DO, Bianco GA, Toscano MA, Salatino M, Vermeulen ME, Geffner JR, and Rabinovich GA. 2009. Tolerogenic signals delivered by dendritic cells to T cells through a galectin-1-driven immunoregulatory circuit involving interleukin 27 and interleukin 10. Nat. Immunol.
33. Mascanfroni ID, Yeste A, Vieira SM, Burns EJ, Patel B, Sloma I, Wu Y, Mayo L, Ben-Hamo R, Efroni S, Kuchroo VK, Robson SC, and Quintana FJ. 2013. IL-27 acts on DCs to suppress the T cell response and autoimmunity by inducing expression of the immunoregulatory molecule CD39. Nat. Immunol.
34. Thom R, Moore JN, Mari ER, Rasouli J, Hwang D, Yoshimura S, Ciric B, Zhang GX, and Rostami AM. 2017. Induction of peripheral tolerance in ongoing autoimmune inflammation requires interleukin 27 signaling in dendritic cells. Front. Immunol.
35. Chihara N, Madi A, Kondo T, Zhang H, Acharya N, Singer M, Nyman J, Marjanovic ND, Kowalczyk MS, Wang C, Kurtulus S, Law T, Etminan Y, Nevin J, Buckley CD, Burkett PR, Buenrostro JD, Rozenblatt-Rosen O, Anderson AC, Regev A, and Kuchroo VK. 2018. Induction and transcriptional regulation of the co-inhibitory gene module in T cells. Nature.
36. Bachem A, Hartung E, Güttler S, Mora A, Zhou X, Hegemann A, Plantinga M, Mazzini E, Stoitzner P, Gurka S, Henn V, Mages HW, and Kroczek RA. 2012. Expression of XCR1 characterizes the Batf3-dependent lineage of dendritic cells capable of antigen cross-presentation. Front. Immunol.
37. Schlitzer A, Sivakamasundari V, Chen J, Bin Sumatoh HR, Schreuder J, Lum J, Malleret B, Zhang S, Larbi A, Zolezzi F, Renia L, Poidinger M, Naik S, Newell EW, Robson P, and Ginhoux F. 2015. Identification of cDC1- and cDC2-committed DC progenitors reveals early lineage priming at the common DC progenitor stage in the bone marrow. Nat. Immunol.
38. Böttcher JP, and Reis e Sousa C. 2018. The Role of Type 1 Conventional Dendritic Cells in Cancer Immunity. Trends in Cancer.
39. Binnewies M, Mujal AM, Pollack JL, Combes AJ, Hardison EA, Barry KC, Tsui J, Ruhland MK, Kersten K, Abushawish MA, Spasic M, Giurintano JP, Chan V, Daud AI, Ha P, Ye CJ, Roberts EW, and Krummel MF. 2019. Unleashing Type-2 Dendritic Cells to Drive Protective Antitumor CD4 + T Cell Immunity. Cell.
40. Ahonen CL, Doxsee CL, McGurran SM, Riter TR, Wade WF, Barth RJ, Vasilakos JP, Noelle RJ, and Kedl RM. 2004. Combined TLR and CD40 Triggering Induces Potent CD8+ T Cell Expansion with Variable Dependence on Type I IFN. J. Exp. Med.
41. Joshi NS, Cui W, Chandele A, Lee HK, Urso DR, Hagman J, Gapin L, and Kaech SM. 2007. Inflammation Directs Memory Precursor and Short-Lived Effector CD8+ T Cell Fates via the Graded Expression of T-bet Transcription Factor. Immunity.
42. Wherry EJ, Ha SJ, Kaech SM, Haining WN, Sarkar S, Kalia V, Subramaniam S, Blattman JN, Barber DL, and Ahmed R. 2007. Molecular Signature of CD8+ T Cell Exhaustion during Chronic Viral Infection. Immunity.
43. Kaech SM, and Wherry EJ. 2007. Heterogeneity and Cell-Fate Decisions in Effector and Memory CD8+ T Cell Differentiation during Viral Infection. Immunity.
44. Olson JA, McDonald-Hyman C, Jameson SC, and Hamilton SE. 2013. Effector-like CD8+ T Cells in the Memory Population Mediate Potent Protective Immunity. Immunity.
45. Herndler-Brandstetter D, Ishigame H, Shinnakasu R, Plajer V, Stecher C, Zhao J, Lietzenmayer M, Kroehling L, Takumi A, Kometani K, Inoue T, Kluger Y, Kaech SM, Kurosaki T, Okada T, and Flavell RA. 2018. KLRG1+ Effector CD8+ T Cells Lose KLRG1, Differentiate into All Memory T Cell Lineages, and Convey Enhanced Protective Immunity. Immunity.
46. Boddupalli CS, Bar N, Kadaveru K, Krauthammer M, Pornputtapong N, Mai Z, Ariyan S, Narayan D, Kluger H, Deng Y, Verma R, Das R, Bacchiocchi A, Halaban R, Sznol M, Dhodapkar MV, and Dhodapkar KM. 2016. Interlesional diversity of T cell receptors in melanoma with immune checkpoints enriched in tissue-resident memory T cells. JCI Insight.
47. Savas P, Virassamy B, Ye C, Salim A, Mintoff CP, Caramia F, Salgado R, Byrne DJ, Teo ZL, Dushyanthen S, Byrne A, Wein L, Luen SJ, Poliness C, Nightingale SS, Skandarajah AS, Gyorki DE, Thornton CM, Beavis PA, Fox SB, Darcy PK, Speed TP, MacKay LK, Neeson PJ, and Loi S. 2018. Single-cell profiling of breast cancer T cells reveals a tissue-resident memory subset associated with improved prognosis. Nat. Med.

48. Corgnac S, Boutet M, Kfoury M, Naltet C, and Mami-Chouaib F. 2018. The emerging role of CD8+ tissue resident memory T (TRM) cells in antitumor immunity: A unique functional contribution of the CD103 integrin. Front. Immunol.

49. Walsh DA, Borges da Silva H, Beura LK, Peng C, Hamilton SE, Masopust D, and Jameson SC. 2019. The Functional Requirement for CD69 in Establishment of Resident Memory CD8 + T Cells Varies with Tissue Location. J. Immunol.

50. Pauken KE, Sammons MA, Odorizzi PM, Manne S, Godec J, Khan O, Drake AM, Chen Z, Sen DR, Kurachi M, Barnitz RA, Bartman C, Bengsch B, Huang AC, Schenkel JM, Vahedi G, Haining WN, Berger SL, and Wherry EJ. 2016. Epigenetic stability of exhausted T cells limits durability of reinvigoration by PD-1 blockade. Science (80-.).

51. Yost KE, Satpathy AT, Wells DK, Qi Y, Wang C, Kageyama R, McNamara KL, Granja JM, Sarin KY, Brown RA, Gupta RK, Curtis C, Bucktrout SL, Davis MM, Chang ALS, and Chang HY. 2019. Clonal replacement of tumor-specific T cells following PD-1 blockade. Nat. Med.

52. Rollins MR, Spartz EJ, and Stromnes IM. 2020. T Cell Receptor Engineered Lymphocytes for Cancer Therapy. Curr. Protoc. Immunol. 129.

53. Pennock ND, Gapin L, and Kedl RM. 2014. IL-27 is required for shaping the magnitude, affinity distribution, and memory of T cells responding to subunit immunization. Proc. Natl. Acad. Sci. U. S. A.

54. Zhang S, Liang R, Luo W, Liu C, Wu X, Gao Y, Hao J, Cao G, Chen X, Wei J, Xia S, Li Z, Wen T, Wu Y, Zhou X, Wang P, Zhao L, Wu Z, Xiong S, Gao X, Gao X, Chen Y, Ge Q, Tian Z, and Yin Z. 2013. High susceptibility to liver injury in IL-27 p28 conditional knockout mice involves intrinsic interferon-γ dysregulation of CD4+ T cells. Hepatology.

55. Huang N, Liu L, Wang XZ, Liu D, Yin SY, and Yang XD. 2008. Association of interleukin (IL)-12 and IL-27 gene polymorphisms with chronic obstructive pulmonary disease in a chinese population. DNA Cell Biol.

56. Barrett JC, Clayton DG, Concannon P, Akolkar B, Cooper JD, Erlich HA, Julier C, Morahan G, Nerup J, Nierras C, Plagnol V, Pociot F, Schuilenburg H, Smyth DJ, Stevens H, Todd JA, Walker NM, Rich SS, Baskerville T, Bautista N, Bhatia E, Bhatia V, Bin Hasan K, Bonnici F, Brodnicki T, Cameron F, Chaichanwatanakul K, Cheung PT, Colman P, Cotterill A, Couper J, Cutfield R, Davis T, Dixon P, Donaghue K, Dowling K, Drury P, Dye S, Gellert S, Abdul Ghani R, Greer R, Han X, Harrison L, Homatopoulos N, Ji L, Jones T, Yin LK, Kamaruddin NA, Kanga U, Kanungo A, Kaur G, Kek B, Knowles S, Krebs J, Kumar N, Lee YJ, Li X, Liktimaskul S, Lloyd M, Loth A, Louey A, Mehra N, Merriman T, Min L, Morahan G, Moses R, Mraz G, Murphy R, Nicholson I, Panelo A, Poh P, Price G, Ratnam N, Sanjeevi C, Sedimbi S, Shen S, Ying GS, Tait B, Tandon N, Thomas A, Varney M, Weerakulwattana P, Willis J, Albret L, Ampudia-Blasco F, Argente J, Babadjanova G, Badenhoop K, Battelino T, Beilhack G, Bergholdt R, Bingley P, Boehm B, Bolidson J, Brorsson C, Carlson J, Castano L, Chandler K, Cinek O, Cipponeri E, Corripio R, Garcia Cuartero B, de Leiva A, Fagulha A, Fernandez Balcells M, Guja C, Gutierrez P, Hatziagelaki E, Heath S, Helmberg W, Hernandez M, Holzheu I, Hosszufalusi N, Ionescu-Tirgoviste C, Johannesen J, Julier C, Kahles H, Knip M, Kockum I, Kojo E, Koprivarova K, Kordonouri O, Kretowski A, Krikovszky D, Kurkhaus A, Lalic N, Lavant E, Long A, Ludvigsson J, Madacsy L, Marga M, Mauricio D, Mazurkievicz G, Nerup J, Novoa Mogollon FJ, Petersen MT, Phillip M, Pirags V, Pociot F, Pozzilli P, Rappner R, Roep B, Rokni S, Rosinger S, Rubio-Cabezas O, Ruckgaber C, Satman I, Schober E, Seufert J, Sing R, Skrha J, Sobngwi E, Somerville M, Spinas G, Tillmann V, Undlien D, Urbanavicius V, Van der Auwera B, Vasquez San Miguel F, Vazeo-Gerasimidi A, Velickiene D, Wagner A, Williams A, Wurzburger M, Ziegler A, Agleham M, Aldrich A, Alemzadeh R, Aly T, Arora S, Austin A, Becker D, Benoist C, Berka N, Bhatia S, Bonella P, Bottini N, Boyle S, Brady B, Brickman W, Christensen R, Concannon P, Couch R, Counts D, Crandall J, Daniels M, Dolan L, Donaldson D, Doria A, Eisenbarth G, El-Hajj R, Erlich H, Fain P, Fear AL, Ferry R, Fiallo-Scharer R, Ghosh S, Gitelman S, Godwin M, Goland R, Goodman N, Goodwin G, Gravely J, Greenbaum C, Gudgeon C, Gunville F, Hagopian W, Hakonarson H, Hansen J, Harrington K, Hassing J, Hilliker W, Hoffman R, Hulbert E, Izquierdo R, Jospe N, Kaiserman K, Kaufman F, Kim S, Kloos E, Kosoy R, Lane J, Lane J, Lawrence J, Levetan C, Levin P, Lipton R, Lonsdale J, Magnuson V, Marks J, Mayer-Davis B, McEvoy R, McIndoe R, Merkle L, Metzger D, Miao D, Mickelson E, Moonsamy P, Moore W, Moran A, Noble J, Olsem G, Onengut-Gumuscu S, Orban T, Orlowski C, Paterson A, Pietropaolo M, Pihoker C, Polychronakos C, Post J, Postellon D,

Pugliese A, Qu H, Quattrin T, Rappaport M, Raskin P, Risbeck H, Rodriguez H, Rodriguez L, Rogers M, Russell B, Schatz D, Scott C, She JX, Shulman D, Soyka L, Speiser P, Starkman H, Steck A, Stender S, Stratton L, Sur D, Taback S, Thrailkill K, Toth E, Trymbiski P, Tsalikian E, Vertachnik K, Wahlen J, Wang X, Weber S, Wherrett D, Willi S, Wilson D, Youkey J, Young N, Yu L, Zimmerman D, Adlem E, Allen J, Brown J, Burren O, Clarke P, Clayton D, Coleman G, Cooper J, Cucca F, Duley S, Dunger D, Everett V, Hardy M, Harrison D, Harrison I, Hawkins S, Healy B, Hood S, Howell S, Maisuria M, Meadows W, Mistry T, Nutland S, Ovington N, Schuilenburg H, Simpson A, Smink L, Stevens H, Taylor N, Todd J, Tuomilehto J, Walker N, Widmer B, Wilson M, Withers H, Brown M, Chen WM, Crews A, Griffin J, Hall M, Harnish T, Hepler J, Hilner J, King N, Lohman K, Lu L, Mychaleckyj J, Nail J, Perdue L, Pierce J, Reboussin D, Rich S, Rushing S, Sale M, Sides E, Snively B, Teuschler H, Theil G, Williams D, Akolkar B, McKeon C, Nierras C, Thomson E, Altshuler D, Au K, Bain S, Barcellos L, Barral S, Becker T, Briggs F, Bronson P, Daly M, de Bakker P, Deloukas P, Devlin B, Eike MC, Field L, Gabriel S, Garge N, Gaudieri S, Goldstein B, Gorodezky C, Hamon S, He C, Howson J, Humphreys K, James I, Lathrop M, Lie BA, Li D, Mack S, McGinnis R, McKinnon E, McLaren W, Nolan D, Olsson M, Ott J, Owerbach D, Patterson C, Podolsky R, Ramsay P, Rangantah V, Risch N, Ronningen KS, Shao X, Single R, Steffes M, Thomson G, Valdes AM, Vandiedonck C, Whittaker P, and Zhang Q. 2009. Genome-wide association study and meta-analysis find that over 40 loci affect risk of type 1 diabetes. Nat. Genet.

57. Devergne O, McFarland EC, Mosialos G, Izumi KM, Ware CF, and Kieff E. 1998. Role of the TRAF Binding Site and NF-κB Activation in Epstein-Barr Virus Latent Membrane Protein 1-Induced Cell Gene Expression. J. Virol.
58. Dibra D, Cutrera JJ, and Li S. 2012. Coordination between TLR9 Signaling in Macrophages and CD3 Signaling in T Cells Induces Robust Expression of IL-30. J. Immunol.
59. Stumhofer JS, and Hunter CA. 2008. Advances in understanding the anti-inflammatory properties of IL-27. Immunol. Lett.
60. Sorrentino C, Ciummo SL, Cipollone G, Caputo S, Bellone M, and Di Carlo E. 2018. Interleukin-30/il27p28 shapes prostate cancer stem-like cell behavior and is critical for tumor onset and metastasization. Cancer Res.
61. Kourko O, Seaver K, Odoardi N, Basta S, and Gee K. 2019. IL-27, IL-30, and IL-35: A Cytokine Triumvirate in Cancer. Front. Oncol.
62. Mirlekar B, Michaud D, Lee SJ, Kren NP, Harris C, Greene K, Goldman EC, Gupta GP, Fields RC, Hawkins WG, DeNardo DG, Rashid NU, Yeh JJ, McRee AJ, Vincent BG, Vignali DAA, and Pylayeva-Gupta Y. 2020. Bcell-derived IL35 drives STAT3-DependentCD8+ T-cell exclusion in pancreatic cancer. Cancer Immunol. Res.
63. Turnis ME, Sawant DV, Szymczak-Workman AL, Andrews LP, Delgoffe GM, Yano H, Beres AJ, Vogel P, Workman CJ, and Vignali DAA. 2016. Interleukin-35 Limits Anti-Tumor Immunity. Immunity.
64. Schenkel JM, and Masopust D. 2014. Identification of a resident T-cell memory core transcriptional signature. Immunol. Cell Biol.
65. Beura LK, Wijeyesinghe S, Thompson EA, Macchietto MG, Rosato PC, Pierson MJ, Schenkel JM, Mitchell JS, Vezys V, Fife BT, Shen S, and Masopust D. 2018. T Cells in Nonlymphoid Tissues Give Rise to Lymph-Node-Resident Memory T Cells. Immunity.
66. Scuteri A, and Monfrini M. 2018. Mesenchymal stem cells as new therapeutic approach for diabetes and pancreatic disorders. Int. J. Mol. Sci.
67. Stromnes IM, Hulbert A, Pierce RH, Greenberg PD, and Hingorani SR. 2017. T-cell localization, activation, and clonal expansion in human pancreatic ductal adenocarcinoma. Cancer Immunol. Res.
68. Peschon JJ, Torrance DS, Stocking KL, Glaccum MB, Otten C, Willis CR, Charrier K, Morrissey PJ, Ware CB, and Mohler KM. 1998. TNF receptor-deficient mice reveal divergent roles for p55 and p75 in several models of inflammation. J. Immunol.
69. MacE TA, Shakya R, Pitarresi JR, Swanson B, McQuinn CW, Loftus S, Nordquist E, Cruz-Monserrate Z, Yu L, Young G, Zhong X, Zimmers TA, Ostrowski MC, Ludwig T, Bloomston M, Bekaii-Saab T, and Lesinski GB. 2018. IL-6 and PD-L1 antibody blockade combination therapy reduces tumour progression in murine models of pancreatic cancer. Gut.

70. Park SL, Buzzai A, Rautela J, Hor JL, Hochheiser K, Effern M, McBain N, Wagner T, Edwards J, McConville R, Wilmott JS, Scolyer RA, Tüting T, Palendira U, Gyorki D, Mueller SN, Huntington ND, Bedoui S, Hölzel M, Mackay LK, Waithman J, and Gebhardt T. 2019. Tissue-resident memory CD8+ T cells promote melanoma–immune equilibrium in skin. Nature.

71. Chopra M, Lang I, Salzmann S, Pachel C, Kraus S, Bäuerlein CA, Brede C, Garrote ALJ, Mattenheimer K, Ritz M, Schwinn S, Graf C, Schäfer V, Frantz S, Einsele H, Wajant H, and Beilhack A. 2013. Tumor Necrosis Factor Induces Tumor Promoting and Anti-Tumoral Effects on Pancreatic Cancer via TNFR1. PLoS One.

72. Zhao X, Fan W, Xu Z, Chen H, He Y, Yang G, Yang G, Hu H, Tang S, Wang P, Zhang Z, Xu P, and Yu M. 2016. Inhibiting tumor necrosis factor-alpha diminishes desmoplasia and inflammation to overcome chemoresistance in pancreatic ductal adenocarcinoma. Oncotarget.

73. Oshima H, Ishikawa T, Yoshida GJ, Naoi K, Maeda Y, Naka K, Ju X, Yamada Y, Minamoto T, Mukaida N, Saya H, and Oshima M. 2014. TNF-/TNFR1 signaling promotes gastric tumorigenesis through induction of Noxo1 and Gna14 in tumor cells. Oncogene.

74. Perez-Ruiz E, Minute L, Otano I, Alvarez M, Ochoa MC, Belsue V, de Andrea C, Rodriguez-Ruiz ME, Perez-Gracia JL, Marquez-Rodas I, Llacer C, Alvarez M, de Luque V, Molina C, Teijeira A, Berraondo P, and Melero I. 2019. Prophylactic TNF blockade uncouples efficacy and toxicity in dual CTLA-4 and PD-1 immunotherapy. Nature.

75. Beyer M, Abdullah Z, Chemnitz JM, Maisel D, Sander J, Lehmann C, Thabet Y, Shinde PV, Schmidleithner L, Köhne M, Trebicka J, Schierwagen R, Hofmann A, Popov A, Lang KS, Oxenius A, Buch T, Kurts C, Heikenwalder M, Fätkenheuer G, Lang PA, Hartmann P, Knolle PA, and Schultze JL. 2016. Tumor-necrosis factor impairs CD4+ T cell-mediated immunological control in chronic viral infection. Nat. Immunol.

76. Badran YR, Cohen JV, Brastianos PK, Parikh AR, Hong TS, and Dougan M. 2019. Concurrent therapy with immune checkpoint inhibitors and TNFα blockade in patients with gastrointestinal immune-related adverse events. J. Immunother. Cancer.

KEY POINTS

- Intratumoral T cells lose IFNγ and GzmB and express elevated Tox and IL10
- Agonistic αCD40 abrogates intratumoral IL27, IL10 and T_{EX}
- αCD40+αPD-L1 and abrogating *Tnfrsf1a* on host cells promotes tumor clearance

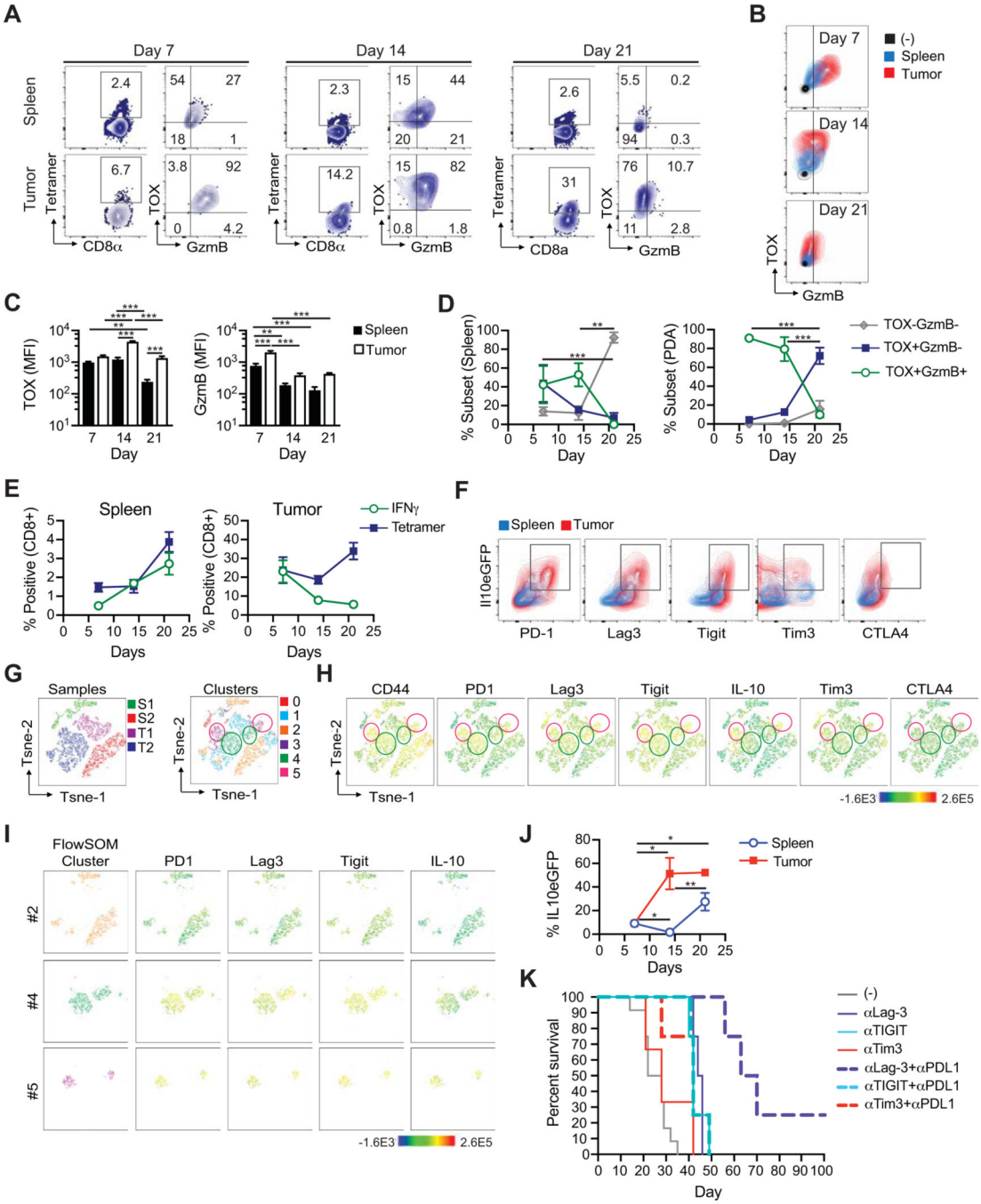

FIGURE 1. Tumor-specific T cells progressively lose Granzyme B and IFNγ while increasing Tox and IL-10 in PDA.

(**A**) Expression of Tox and GzmB gated on $CB_{101–109}$:$H2D^b$ tetramer+ CD8 T cells. n=4–5 mice per timepoint. (**B**) Overlay of GzmB in splenic and intratumoral tetramer+ T cells over time. (–), no intracellular stain control. n=4–5 mice per group. (**C**) Mean fluorescence intensity (MFI) of Tox (left) and GzmB (right) in $CB_{101–109}$:$H2D^b$ tetramer+ CD8 T cells. Data are mean ± S.E.M. **, p<0.005, unpaired two-tailed student's T test. n=4–5 mice per group. (**D**) Proportion of $CB_{101–109}$:$H2D^b$ tetramer+ CD8 T cells in spleen (left) and tumor

(right) positive for Tox and/or GzmB. Data are mean ± S.E.M. n=4–5 mice per group. (**E**) Proportion of splenic (left) or intratumoral tumor (right) CD8+ T cells that produce IFNγ in response to ex vivo $CB_{101–109}$ peptide re-stimulation and/or bind $CB_{101–109}$:$H2D^b$ tetramer over time. Data are mean ± S.E.M., n=3–5 mice per time point. (**F**) Proportion of CD8+tetramer+ T cells that are positive for eGFP on day 21 post orthotopic tumor implantation into $Il10^{eGFP}$ tumor-bearing mice. (**G**) An unbiased FlowSOM Tsne analysis was performed on CD8+tetramer+ T cells in concatenated spleen and tumors from 2 independent *KPC*2a-tumor bearing mice on day 21 post orthotopic tumor implantation. Left plot: Tsne plot specifying sample location where each dot is a single CD8+tetramer+ T cell. S1, spleen 1; S2, spleen 2; T1, tumor 1; T2, tumor 2. Right plot: The 6 clusters (C0-C5) were identified by a FlowSOM algorithm plugin for Flowjo, where each cell of the 4 samples was assigned to one of 6 clusters based on expression of CTLA4, Tim3, Lag3, Tigit, IL-10, and PD1. (**H**) Marker intensity in cell clusters from Figure 1G. Pink circles, cluster 5. (**I**) An unbiased FlowSOM algorithm identified 6 clusters based on tetramer+ CD8 T cell expression of CTLA4, Tim3, Lag3, Tigit, IL-10, and PD1 in all 4 samples. Marker intensity shows high IL-10 in cluster 5. (**J**) Expression of IL-10 in CD8+ tetramer+ T cells over time in *KPC*2a tumor-bearing $IL\text{-}10^{eGFP}$ reporter mice was determined by flow cytometric analysis of GFP. *, $p<0.05$, **, $p<0.005$. One-way Anova with a Tukey post-test. (**K**) Kaplan-Meier survival curve of tumor-bearing mice treated αLag3 (clone C9B7W), αTim3 (RMT3–23) or αTIGIT (clone 1G9) alone or in combination with αPD-L1 (10F.9G2). αLAG3 significantly prolonged survival compared to controls ($p=0.0011$). αLAG3+αPD-L1 significantly prolonged survival compared to αLAG3 alone ($p=0.0091$). αTigit significantly prolonged survival compared to controls ($p=0.0035$). Asterisks indicate significant differences compared to control mice. Significance was determined by a Log-rank (Mantel-cox) test. n=4–10 mice per group.

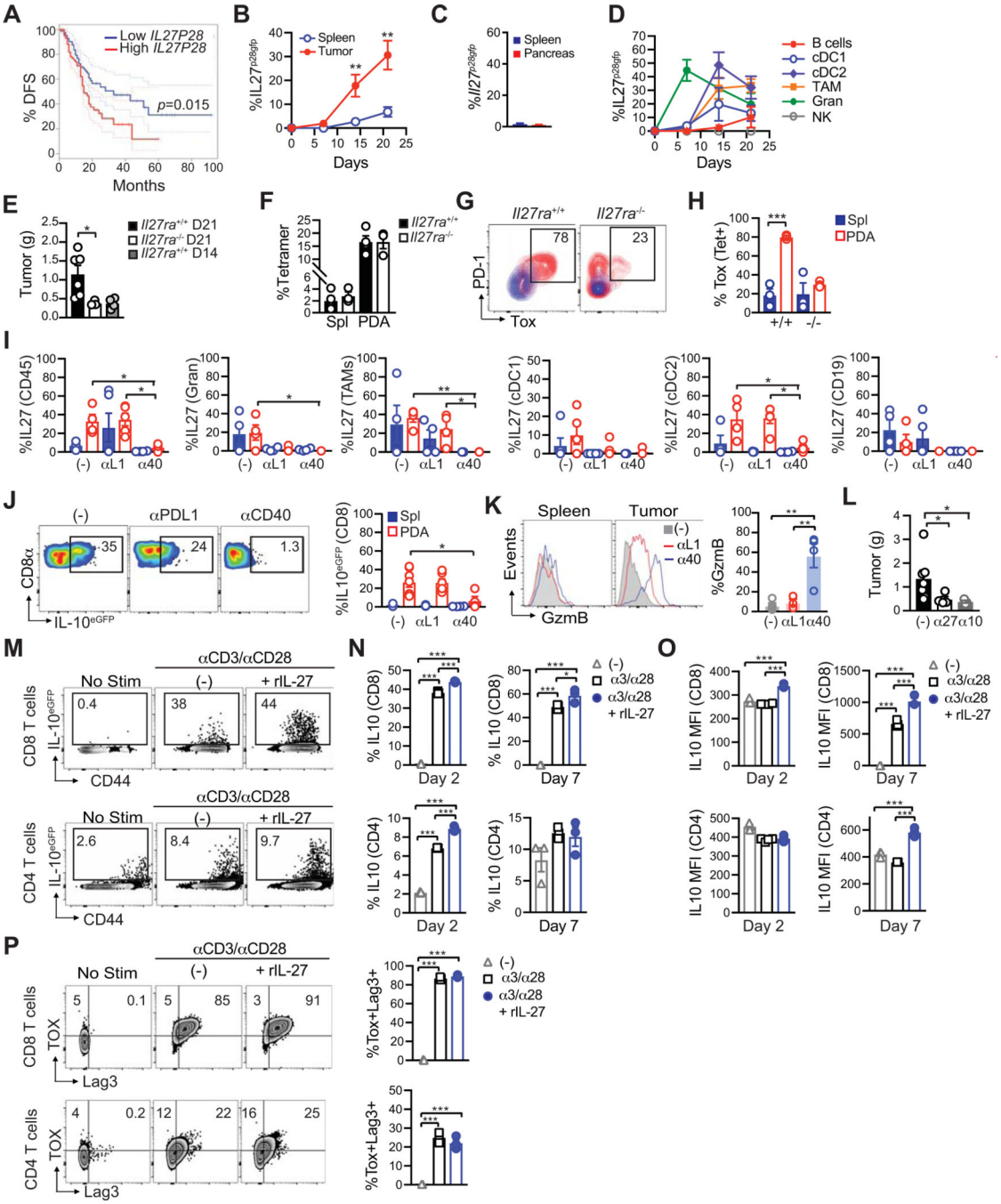

FIGURE 2. Agonistic αCD40 abrogates intratumoral myeloid cell production of IL-27 and T_{EX} formation.

(**A**) Disease-free survival (DFS) in PDA patients with tumors that express high (n=89) or low (n=89) *IL27P28.* Graph was generated using the GEPIA (http://gepia.cancer-pku.cn/). Significance was determined by a log-rank test. (**B**) Proportion of CD45+ cells that are GFP + following orthotopic *KPC*2a tumor cell injection into *Il27p28*^{eGFP}mice. Data are mean ± S.E.M. **, $p<0.005$, unpaired two-tailed student's T test. n=3–5 mice per timepoint. (**C**) Proportion spleen- or pancreas-residing CD45+ cells that are GFP+ from untreated

Il27p28^{egfp} reporter mice. Data are mean ± S.E.M. n=4 mice per group. (**D**) Proportion of the indicated intratumoral immune cell subsets that express GFP. Cells were prepared from *KPC*2a orthotopic tumors isolated from *Il27p28*^{eGFP} mice and gated accordingly to Supplemental Fig. 2B. Data are mean ± S.E.M. n=3–5 mice per timepoint. (**E**) Tumor weight in grams from *Il27ra*$^{+/+}$ at either day 14 (D14) or day 21 (D21) and *Il27ra*$^{-/-}$ mice at day 21 (D21) post tumor implantation. Data are mean ± S.E.M. *, $p<0.05$, one-way ANOVA with a Tukey's post-test. n=4–6 mice per group. (**F**) Proportion of splenic (Spl) or intratumoral (PDA) CD8+ T cells that bind $CB_{101–109}$-H2-D^b tetramer on day 21 post tumor implantation in *Il27ra*$^{+/+}$ and *Il27ra*$^{-/-}$ mice. Each dot is an independent mouse. Data are mean ± S.E.M. n=3–5 mice per group. (**G**) Representative PD-1 and Tox staining in CD8+tetramer+ T cells isolated from spleen (blue) or tumor (red) from *Il27ra*$^{+/+}$ (+/+, day 14) or *Il27ra*$^{-/-}$ mice (−/−, day 21). Tumors were harvested at different timepoints to normalize for tumor size. (**H**) Quantification of Fig. 2G. Data are mean ± S.E.M. Each dot is an independent mouse. ***, $p<0.0005$, two-tailed unpaired student's T test comparing spleen vs. tumor. n=3–4 mice per group. (**I**) Proportion of cell subsets that express GFP in untreated (–), αPD-L1 (αL1), or αCD40 (α40)-treated *Il27p28*^{eGFP}-reporter animals. Mononuclear cells were prepared from *KPC*2a orthotopic tumors (PDA) or spleen (Spl) harvested from *Il27p28*^{eGFP} mice on day 21 post tumor implantation. Data are mean ± S.E.M. n=3–5 mice per group. *, $p<0.05$; **, $p<0.005$, one-way ANOVA with a Tukey's post-test. (**J**) Representative flow cytometry plots of intratumoral CD8+ T cells isolated from tumors isolated from untreated (–), αPD-L1- (αL1), or αCD40 (α40)-treated *Il10*^{eGFP} mice on day 21. Plots are quantified data. Each dot is an independent animal. Data are mean ± S.E.M. n=3–5 mice per group. *, $p<0.05$, one-way ANOVA with a Tukey's post-test. (**K**) Histogram overlays (left) and quantification (right) of GzmB in splenic or intratumoral $CB_{101–109}$:H-$2D^b$-specific CD8+ T cells on day 14 post tumor implantation. Data are mean ± S.E.M. Each dot is an independent mouse. **$p<0.005$, one-way ANOVA with a Tukey's post-test. n=3–5 mice per group. (**L**) Tumor weight in grams (g) from tumor-bearing B6 mice treated with αIL-10R or αIL27p28 as depicted in Supplementary Fig. 2H. n=4–7 mice per group. Each dot is an independent animal. Data are mean ± S.E.M. *, $p<0.05$, one-way ANOVA with a Tukey's post-test. (**M**) Flow cytometry plots gated on CD8 (top row) and CD4 (bottom row) T cells isolated from the spleens of *Il10*^{eGFP} reporter mice following *in vitro* activation with αCD3 + αCD28 ± recombinant murine IL-27 (rIL-27) for 2 days. Control cells were left unstimulated (No Stim). (**N**) Proportion of CD8 (top row) and CD4 (bottom row) T cells that are GFP+ on day 2 or day 7 post *in vitro* activation as in Fig. 2M. Data are mean ± S.E.M. Each dot is a technical replicate. *$p<0.05$, ***$p<0.0005$, one-way ANOVA with a Tukey's post-test. (**O**) MFI of GFP in CD8 (top row) and CD4 (bottom row) T cells on day 2 or day 7 post *in vitro* activation as in Fig. 2M. Data are mean ± S.E.M. Each dot is a technical replicate. ***$p<0.0005$, one-way ANOVA with a Tukey's post-test. (**P**) Flow cytometry plots of Tox and Lag3 expression gated on CD8 (top row) and CD4 (bottom row) T cells isolated from the spleens of *Il10*^{eGFP} reporter mice following *in vitro* activation with αCD3 + αCD28 ± rIL-27 for 7 days. Proportion of CD8 (top) and CD4 (bottom) T cells that co-express Lag3 and Tox on day 7. Data are mean ± S.E.M. Each dot is a technical replicate. ***$p<0.0005$, one-way ANOVA with a Tukey's post-test.

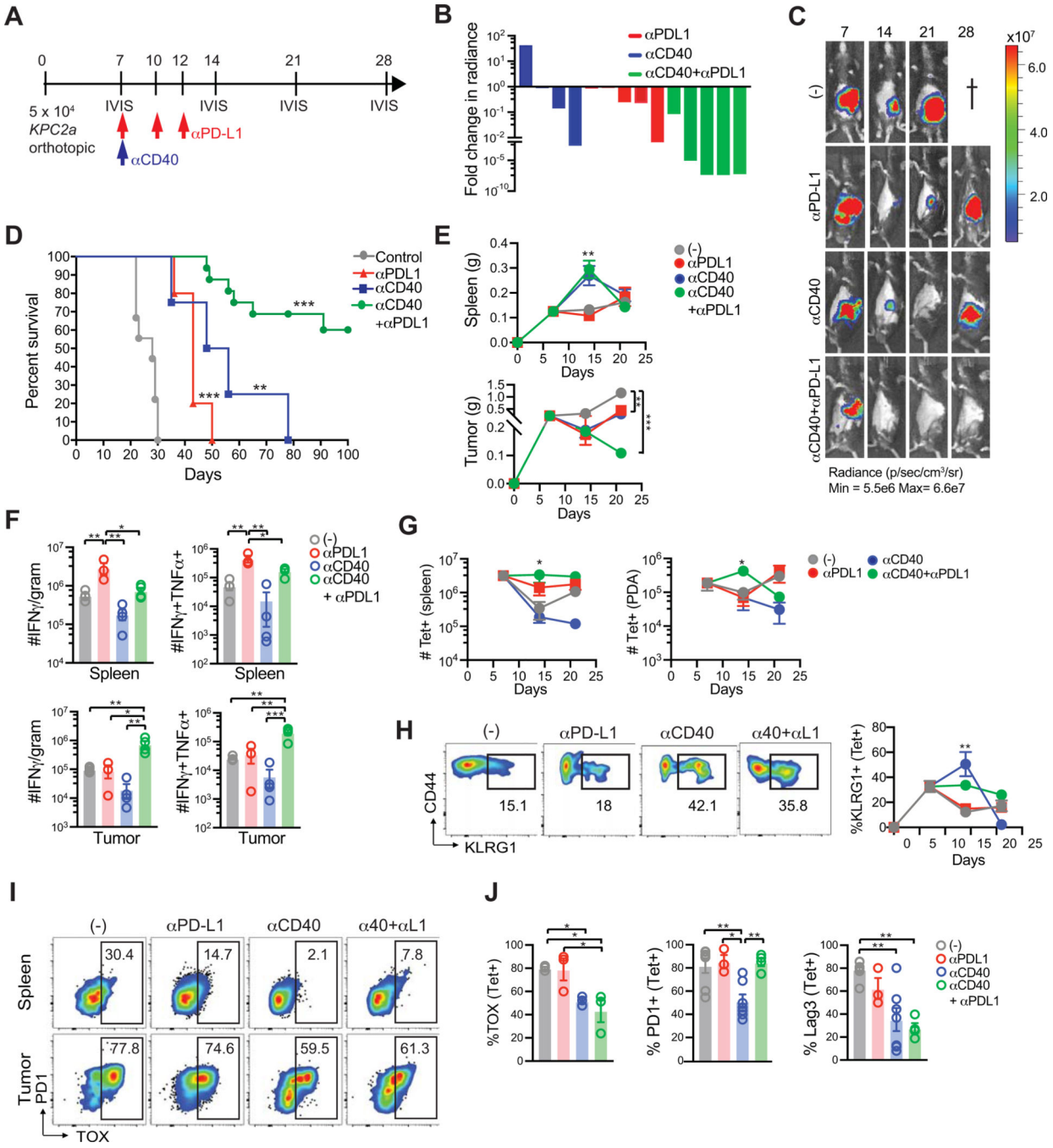

Figure 3. Agonistic αCD40 and αPD-L1 blockade promote pancreatic cancer eradication.

(**A**) Schematic for testing αPD-L1, αCD40 or the combination following tumor implantation. (**B**) Fold change in tumor radiance 3 weeks post immunotherapy initiation was determined by IVIS imaging. Each bar is an independent mouse. n=4–5 mice per group. (**C**) Representative tumor radiance from a single mouse from each experimental cohort treated as shown in Figure 3B. Representative of n=4–5 mice per group. †, euthanasia required due to tumor growth on day 21. (**D**) Kaplan-Meier survival curve of tumor-bearing mice treated αPD-L1, agonistic αCD40 or the combination as shown in Figure 3A. Agonistic

αCD40+αPD-L1 significantly prolonged survival compared to controls (p<0.0001), αPD-L1 monotherapy (p<0.0001), and αCD40 monotherapy (p=0.0028). αCD40 or αPD-L1 significantly prolonged survival compared to control animals (p=0.0021 and p<0.0001, respectively). Control animals include both untreated (n=6) and isotype treated (n=3) mice. A statistically significant difference was not detected between αCD40 vs. αPD-L1 cohorts (p=0.0690). Asterisks indicate significant differences compared to control mice and significance was determined by a Log-rank (Mantel-cox) test. n=4–16 mice per group. (**E**) Spleen and tumor weights following αCD40, αPD-L1 or the combination in tumor-bearing mice. Mice received αCD40, αPD-L1 or the combination as in Figure 3A. On day 14, αCD40 alone, or αCD40+αPD-L1, significantly increased spleen weight compared to control and αPD-L1 cohorts (**p<0.005). By day 21, αPD-L1+αCD40 (***p<0.0005), αPD-L1 (**p<0.005) or αCD40 (**p<0.005) significantly decreased tumor weight compared to untreated (–) mice. Significance was determined by a one-way ANOVA with a Tukey's multiple comparison test. Data are mean ± S.E.M. n=4–7 mice per group. (**F**) Number of intratumoral IFNγ+ (left graph) or IFNγ+TNFα+-producing CD8+ T cells following a 4-hour ex vivo incubation with $CB_{101–109}$ peptide. Cytokine staining was determined by intracellular cytokine staining and flow cytometry. Cell numbers are normalized to spleen and tumor gram. Data are mean ± S.E.M. *p<0.05, **p<0.005, ***p<0.0005. Significance was determined by a one-way ANOVA with a Tukey's post-test. n=3–5 mice per group. (**G**) Number of splenic and intratumoral $CB_{101–109}$:H-$2D^b$-specific CD8+ T cells normalized to tissue gram in tumor-bearing mice following αPD-L1, αCD40 or the combination. Data are mean ± S.E.M. αCD40+αPD-L1 significantly increased tumor-specific T cell number in spleen and tumor on day 14 compared to untreated or αCD40 cohorts, **p<0.005, one-way ANOVA with a Tukey's post-test. n=4–7 mice per group. (**H**) Representative flow cytometry plots for CD44 and Klrg1 gated on live, CD8+tetramer+ T cells on day 14 (left) and proportion of intratumoral CD8+tetramer+ T cells that express KLRG1 over time (right). Data are mean ± S.E.M. On day 14, αCD40 or αCD40+αPD-L1 significantly increased the proportion of intratumoral CD8+tetramer+ T cells that expressed Klrg1. **p<0.005. Significance was determined for both graphs by a one-way ANOVA and Tukey's multiple comparison test. n=4–7 mice per group. (**I**) Representative flow cytometry plots for PD-1 and Tox gated on CD8+tetramer+ T cells on day 14. n=3–4 mice per group. (**J**) Proportion of intratumoral CD8+tetramer+ T cells that express Tox, PD-1 or Lag-3 on day 14. Data are mean ± S.E.M. Each dot is an independent mouse. *p<0.05, **, p<0.005, one-way ANOVA with a Tukey's post-test. n=3–6 mice per group.

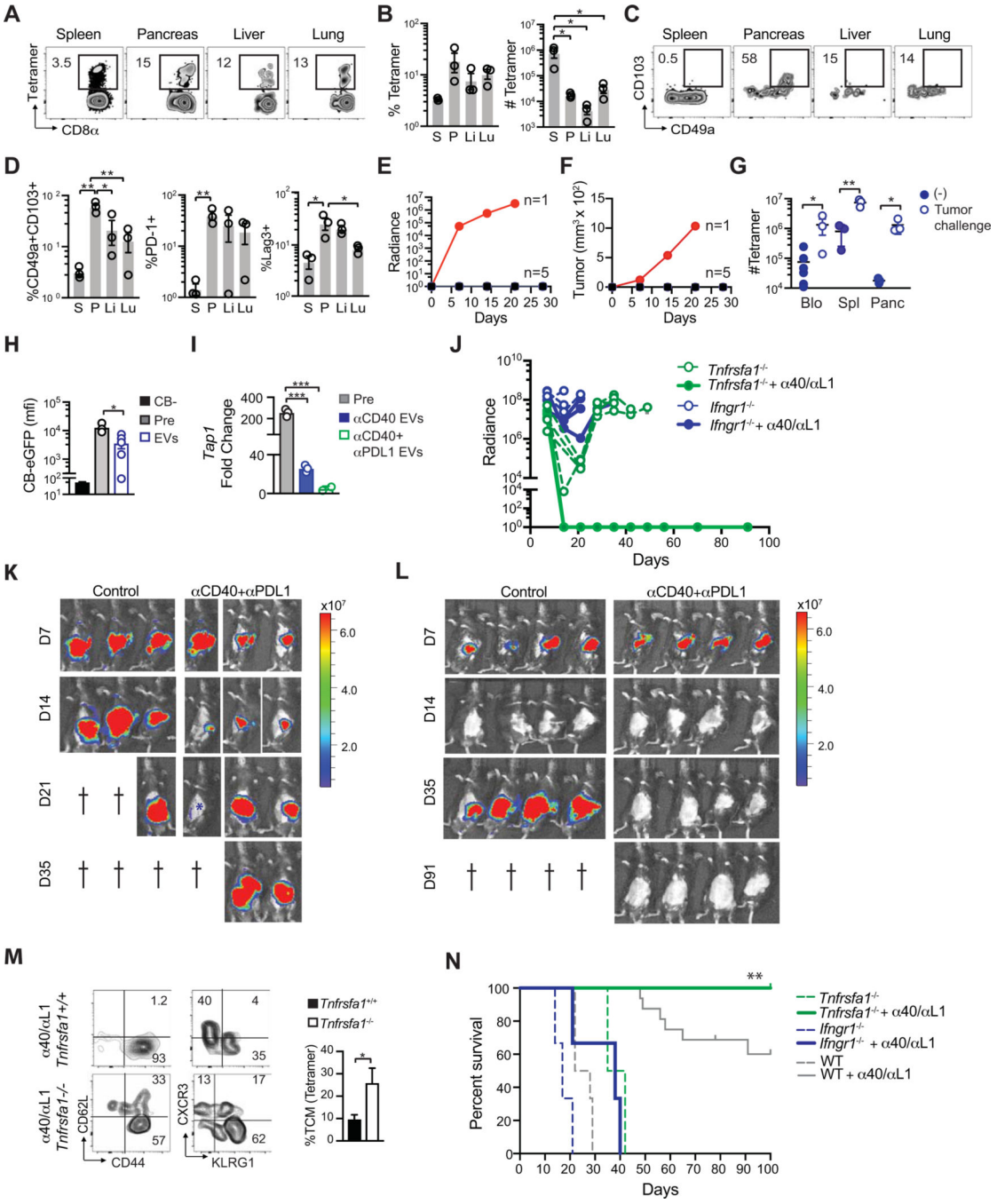

Figure 4. Interfering with *Tnfrsfa1* in host cells overcomes tumor escape following αCD40+αPD-L1

(**A**) Plots of CD8+tetramer+ T cells isolated from the indicated tissues at ~3 months following αCD40+αPD-L1 gated on live CD8+ T cells. (**B**) Proportion (left graph) and number (right graph) of CD8+tetramer+ T cells in spleen (S), pancreas (P), liver (Li) and lung (Lu). Cell numbers are normalized to tissue gram. Data are mean ± S.E.M. Each dot is an independent animal. *p<0.05, one-way ANOVA with a Tukey's multiple comparison test. n=3 mice per group. (**C**) Representative CD103 and CD49a expression gated on

CD8+tetramer+ T cells ~3 months' post tumor challenge and αCD40+αPD-L1 therapy. Numbers are the frequency of tetramer+ T cells that co-express CD103 and CD49a. (**D**) Proportion of CD8+tetramer+ T cells that express CD49a and CD103, PD-1, Lag3 in spleen (S), pancreas (P), liver (Li) and lung (Lu). Data are mean ± S.E.M. Each dot is an independent animal. *p<0.05, one-way ANOVA with a Tukey's multiple comparison test. n=3 mice per group. (**E**) Tumor radiance was determined by IVIS imaging following orthotopic *KPC*2a re-challenge (n=3) or 9:1 mixture of *KPC*2a CB+ with parental *KPC*2 CB-negative tumor (n=3) on day 100 post αCD40+αPD-L1. Red line, a recipient of the 9:1 CB+:CB- tumor with tumor outgrowth (see Figures S4E and S4F for tumor images). (**F**) Tumor volume of the identical animals in Figure 4E (n=6) was determined also by high-resolution ultrasound to quantify tumor volume independent of CB expression. Red line, one of the recipients (mouse #5) of the 9:1 tumor combination had an outgrowth of CB- tumor (see Figures S4H and S4I). (**G**) Number of CD8+tetramer+ cells in blood (Bl), spleen (Spl) and normal pancreas (Panc) from αCD40+αPD-L1-cured animals on day 100, or, 30 days following orthotopic tumor re-challenge from mice. Cell numbers are normalized to tissue gram or milliliter. Data are mean ± S.E.M. Each dot is an independent animal. *p<0.05, **p<0.005, unpaired two-tailed student's T test. (**H**) Mean fluorescence intensity (mfi) of tumor cell CB-eGFP was determined by flow cytometry. CB-, parental *KPC* cell line and negative control; Pre, *KPC*2a CB+ cell line prior to tumor implantation; EVs, escape variants from 5 independent animals treated with αCD40 (n=3) or αCD40+αPD-L1 (n=2). Data are mean ± S.E.M. Each dot is an independent animal. *p<0.05, unpaired two-tailed student's T test. (**I**) Fold change in *Tap1* induction in *KPC*2a cells prior to implantation (Pre) and EVs (from Fig. 4H, n=5) 48 h following recombinant IFNγ incubation, was determined by qPCR and normalized to the housekeeping gene *Atp5b*. **p<0.005, ANOVA, with a Tukey's post-test. Each dot is a biological replicate, reflecting the mean of technical replicates performed in triplicate. (**J**) Calculation of tumor radiance (p/sec/cm^2/sr) from animals in Fig. 4K and 4L was determined by IVIS. Each line is an independent animal. (**K**) Tumor bioluminescent images in control or αCD40+αPD-L1-treated *Ifngr1*$^{-/-}$ mice. †, euthanasia due to tumor growth; asterisk, tumor lost CB-eGFP and therefore was not detected by IVIS (not shown). (**L**) Tumor bioluminescent images in control or αCD40+αPD-L1-treated *Tnfrsfa1*$^{-/-}$ mice. (**M**) Representative flow cytometric staining of effector and memory markers expressed by circulating CD8+tetramer+ T cells in cured animals ~80–90 days after tumor implantation. Plots are gated on CD8+tetramer+ T cells and quantified in the graph. Data are mean ± S.E.M. n=4 mice per group. Each dot is an independent animal. *p<0.05, unpaired two-tailed student's T test. (**N**) Kaplan-Meier survival curve of *KPC*2a orthotopic tumor-bearing *Ifngr*$^{-/-}$ or *Tnfrasf1*$^{-/-}$ mice treated with isotype, or αCD40+αPDL1. Combination αCD40+αPDL1 significantly prolonged *Tnfrasf1*$^{-/-}$ mouse survival compared to control *Tnfrasf1*$^{-/-}$ mice (p=0.0084). αCD40+αPDL1 trended to prolong survival in *Ifngr1*$^{-/-}$ mice (p=0.063). Control *Tnfrasf1*$^{-/-}$ mice survived significantly longer than control *Ifngr*$^{-/-}$ mice (p=0.0101). Statistical significance was determined by a Log-rank (Mantel-cox) test. Wild type mouse survival curves are identical to wild type curves in Figure 3D.